

# Development of High Performance MEMS Accelerometer for Inertial Navigation



Muhammad Ameer Umar Malik  
Regn Number: NUST201261241MCEME35512F

Supervisor

Dr. Umer Izhar

DEPARTMENT OF MECHATRONICS ENGINEERING  
COLLEGE OF ELECTRICAL & MECHANICAL ENGINEERING  
NATIONAL UNIVERSITY OF SCIENCES AND TECHNOLOGY  
ISLAMABAD

\_\_\_\_ April, 2016

Development of High Performance MEMS Accelerometer for Inertial  
Navigation

Muhammad Ameer Umar Malik

NUST201261241MCEME35512F

A thesis submitted in partial fulfillment of the requirements for the degree of  
MS Mechatronics Engineering

Thesis Supervisor:

Dr. Umer Izhar

Thesis Supervisor's Signature: \_\_\_\_\_

DEPARTMENT OF MECHATRONICS ENGINEERING  
COLLEGE OF ELECTRICAL & MECHANICAL ENGINEERING  
NATIONAL UNIVERSITY OF SCIENCES AND TECHNOLOGY,  
ISLAMABAD

\_\_\_\_ April, 2016

## **Declaration**

I certify that this research work titled “*Development of High Performance MEMS Accelerometer for Inertial Navigation*” is my own work. The work has not been presented elsewhere for assessment. The material that has been used from other sources it has been properly acknowledged / referred.

Signature of Student

M. Ameer Umar Malik

2016-NUST-Ms-MTS-74

NUST201261241MCEME35512F

## **Language Correctness Certificate**

This thesis has been read by an English expert and is free of typing, syntax, semantic, grammatical and spelling mistakes. Thesis is also according to the format given by the University.

Signature of Student

M. Ameer Umar Malik

NUST201261241MCEME35512F

Signature of Supervisor

## **Copyright Statement**

- Copyright in text of this thesis rests with the student author. Copies (by any process) either in full, or of extracts, may be made only in accordance with instructions given by the author and lodged in the Library of NUST College of E&ME. Details may be obtained by the Librarian. This page must form part of any such copies made. Further copies (by any process) may not be made without the permission (in writing) of the author.
- The ownership of any intellectual property rights which may be described in this thesis is vested in NUST College of E&ME, subject to any prior agreement to the contrary, and may not be made available for use by third parties without the written permission of the College of E&ME, which will prescribe the terms and conditions of any such agreement.
- Further information on the conditions under which disclosures and exploitation may take place is available from the Library of NUST College of E&ME, Rawalpindi.

## **Acknowledgements**

I am thankful to my Creator Allah Subhana-Watala to have guided me throughout this work at every step and for every new thought which Allah setup in my mind to improve it. Indeed I could have done nothing without Allah's priceless help and guidance. Whosoever helped me throughout the course of my thesis, whether my parents or any other individual was Allah's will, so indeed none be worthy of praise but Allah.

I am profusely thankful to my beloved parents who raised me when I was not capable of walking and continued to support me throughout in every department of my life.

I would also like to express special thanks to my supervisor Dr. Umer Izhar for his help throughout my thesis and also for MEMS course which he has taught me. I can safely say that I have in depth understanding of this subject.

I would also like to thank Dr. Kunwar Faraz Ahmad, Dr. Umar Shahbaz, and Dr. Himayat Ullah for my thesis guidance and evaluation, and express my special thanks to Dr. Mubashir Saleem for his guidance as PG coordinator. I am also thankful to Mr. Zahid for his support and cooperation.

Finally, I would like to express my gratitude to all the individuals who have rendered valuable assistance to my study.

*Dedicated to my exceptional parents and adored siblings whose  
tremendous support and cooperation led me to this wonderful  
accomplishment*

## Abstract

Accelerometer is an important sensor of inertial navigation system. Focus of new developments is a low cost, small size sensor with high performance that meets the requirements of navigation. In this research work a multi wafer magnetic MEMS accelerometer design is proposed and analyzed for inertial navigation. Capacitive pick off is used to sense deflection of sensor mass and permanent magnet & coil is used for rebalancing of deflected mass of the sensor. System steady state sensitivity is 1mA/g which means that means 1mA is required to balance the force of 1 g input on the proof mass of this sensor when operated in a close loop system. System is designed to measure the input acceleration up to  $\pm 10g$  with resolution of  $10\mu g$ . Total capacitive area of sensor is  $11 \text{ mm}^2$  with gap of  $10 \mu\text{m}$  and capacitive pickoff coefficient is designed to be 6635 pF/rad. Permanent magnet with thickness of  $330 \mu\text{m}$  and radius of  $700 \mu\text{m}$  and soft magnet material coating is used. Out of plane coil with total 144 turns, 12 layers and cross-section area  $20\mu\text{m} \times 20\mu\text{m}$  is used. Fabrication process outlines for both, the magnetic system and coils are proposed separately. Stress analysis for flexures of sensing pendulum has been carried out. Close loop frequency response analysis is carried out with a proposed PID controller.

**Key Words:** *Magnetic MEMS, Accelerometer*



## Table of Contents

<b>Declaration .....</b>	<b>i</b>
<b>Language Correctness Certificate.....</b>	<b>ii</b>
<b>Copyright Statement .....</b>	<b>iii</b>
<b>Acknowledgements .....</b>	<b>iv</b>
<b>Abstract .....</b>	<b>vi</b>
<b>Table of Contents.....</b>	<b>vii</b>
<b>List of Figures .....</b>	<b>ix</b>
<b>List of Tables.....</b>	<b>x</b>
<b>CHAPTER 1: INTRODUCTION.....</b>	<b>1</b>
1.1    Background, Scope and Motivation .....	1
1.1.1    Motivation & Scope.....	1
1.2    Accelerometer Introduction.....	2
1.2.1    Performance Parameters .....	2
1.3    MEMS Accelerometers .....	3
1.3.1    Transduction Mechanisms .....	4
1.3.2    MEMS Accelerometers History.....	6
1.4    Navigation Grade Accelerometer.....	8
<b>CHAPTER 2: MAGNETS IN MEMS .....</b>	<b>11</b>
2.1    Magnetics Materials .....	11
2.1.1    Hard Magnets.....	11
2.1.2    Soft Magnets.....	12
2.2    Challenges for use of Hard Magnets in MEMS .....	12
2.2.1    Fabrication of Magnets in MEMS .....	13
2.3    Future of Magnets in MEMS .....	14
<b>CHAPTER 3: ANALYTICAL MODEL AND PROPOSED DESIGN .....</b>	<b>15</b>
3.1    Analytical Model of Accelerometer Working Principle.....	15
3.2    Proposed Design Outline.....	17
<b>CHAPTER 4: MODELING OF DESIGN PARAMETERS .....</b>	<b>20</b>
4.1    Parameter Estimation of Flexure Part .....	20
4.1.1    Spring Constant / Stiffness of Hinge Estimation: .....	20
4.1.2    Moment of Inertia Calculation:.....	22
4.1.3    Damping Coefficient Estimation: .....	23
4.2    Close loop System Model &Parameters Estimation .....	24
4.2.1    Pickoff Angle Sensor - $H_{PA}$ (pF/rad) .....	25
4.2.2    Torquer Moment Transfer Function - HTM in g-mm/A.....	26

4.2.3	Pickoff Sensor Amplifier Transfer Function - $H_{PSA}$ in V/ pF & Control Amplifier - $H_{CA}$ in A/V .....	27
<b>CHAPTER 5: DESIGN AND STRUCTURAL ANALYSIS .....</b>	<b>29</b>	
5.1	Structure Analysis .....	29
5.1.1	Analytical Structure Analysis .....	29
5.1.2	FEM Analysis .....	32
5.2	Magnetic Field Analysis .....	32
5.2.1	Magnetic Field .....	33
5.2.2	Coil Placement.....	37
<b>CHAPTER 6: FABRICATION PROCESSES .....</b>	<b>40</b>	
6.1	Magnet Fabrication .....	40
6.2	Flexure Fabrication .....	41
6.3	Flexure Fabrication Stiffness Results.....	42
6.4	Coil Fabrication.....	43
<b>CHAPTER 7: CONTROL ANALYSIS .....</b>	<b>46</b>	
7.1	Close Loop Operation with Controller .....	46
7.2	Deflection Analysis.....	50
7.3	Comparison with Other Devices .....	51
<b>CONCLUSION .....</b>	<b>52</b>	
<b>FUTURE WORK.....</b>	<b>52</b>	
<b>APPENDIX A.....</b>	<b>53</b>	
<b>REFERENCES .....</b>	<b>56</b>	

## List of Figures

<b>Figure 1.1:</b> Mechanical structure design of the vertical axis accelerometer [15].	7
<b>Figure 1.2:</b> Structure of out of plane capacitive MEMS accelerometer by Colibrys [17]	8
<b>Figure 1.3:</b> Comparison of few commercial MEMS accelerometers [4].	8
<b>Figure 1.4:</b> Accelerometer performance requirement for different applications [3].	10
<b>Figure 3.1:</b> Accelerometer working principle	15
<b>Figure 3.2:</b> Close loop accelerometer working principle	16
<b>Figure 3.3:</b> Block diagram of close loop system	17
<b>Figure 3.4:</b> Three wafer design diagram	18
<b>Figure 3.5:</b> Three wafer fabricated device (without coils & magnet)	18
<b>Figure 3.6:</b> Analytical model of proposed design	19
<b>Figure 4.1:</b> Three wafer design model	20
<b>Figure 4.2:</b> Design parameter dimensions	21
<b>Figure 4.3:</b> Complete system model	24
<b>Figure 5.1:</b> Static condition when centre wafer is free.	29
<b>Figure 5.2:</b> Static equilibrium condition when centre wafer is fixed between two wafers.	31
<b>Figure 5.3:</b> FEM stress analysis for free condition	32
<b>Figure 5.4:</b> Three different magnet system configurations	33
<b>Figure 5.5:</b> ThreeSurface Plot of Magnetic Field	34
<b>Figure 5.6:</b> Surface plot of magnetic field	35
<b>Figure 5.7:</b> Magnet flux density along 'z' direction at $r = 700 \mu\text{m}$	35
<b>Figure 5.8:</b> Magnet flux density (configuration-iii) in radial 'r' direction at $z = 200 \mu\text{m}$ from centre of magnet	36
<b>Figure 5.9:</b> Soft Magnet Thickness and Magnetic Field Variation	37
<b>Figure 5.10:</b> Force direction and distance parameter 'XX'	38
<b>Figure 5.11:</b> Force on coil, three different configurations	38
<b>Figure 5.12:</b> Surface Plot of Magnetic Field	39
<b>Figure 6.1:</b> Magnet Fabrication process description	41
<b>Figure 6.2:</b> Flexure wafer fabrication processes (i) Etching / cutting of proof mass profile. (ii) Etching of two flexures. (iii) Thin film plating of capacitive area and connections.	42
<b>Figure 6.3:</b> Coil fabrication processes	44
<b>Figure 6.4:</b> Three wafers and device	45
<b>Figure 7.1:</b> Close loop architecture with output configuration	47
<b>Figure 7.2:</b> Frequency response plot of closed loop architecture	47
<b>Figure 7.3:</b> Step response of close loop architecture	48
<b>Figure 7.4:</b> Response of close loop architecture at 100 Hz	48
<b>Figure 7.5:</b> Input signal at 100 Hz with multiple 'g' steps	49
<b>Figure 7.6:</b> Response of system to Input signal at 100 Hz with multiple 'g' steps	49
<b>Figure 7.7:</b> Close loop architecture for angular deflection	50
<b>Figure 7.8:</b> Deflection of sensor against step input	50

## List of Tables

<b>Table 1-1:</b> Typical specifications of accelerometers for automotive and inertial navigation applications [6].....	9
<b>Table 1-2:</b> Target performance parameters for navigation grade accelerometer .....	10
<b>Table 4-1:</b> Design parameters dimension values .....	21
<b>Table 5-1:</b> Structure parameters of centre wafer.....	30
<b>Table 5-2:</b> Simulation parameters .....	33
<b>Table 6-1:</b> Stiffness test results .....	43
<b>Table 7-1:</b> Close loop control system parameters .....	46
<b>Table 7-2:</b> Performance comparison with other devices .....	51

# **CHAPTER 1: INTRODUCTION**

The research work focuses on the design of a magnetic MEMS navigation grade accelerometer. Motivation and scope for this work is briefly described. A brief introduction of accelerometer with its performance parameters is given. Also an introduction of MEMS accelerometers with brief history of their development and performance as presented by researchers and companies is stated. Performance requirements for navigation grade accelerometers are discussed at the end as a reference for design requirement.

## **1.1 Background, Scope and Motivation**

For inertial navigation of any system high performance accelerometers are required. Traditionally high accuracy electromechanical accelerometers are used for this purpose. But for small applications where weight is very critical MEMS accelerometers are required. Performance of commercial of the shelf available MEMS accelerometers is not enough for high accuracy requirements. Purpose of this work is to design a MEMS accelerometer that can meet the performance requirements of a high accuracy inertial measuring unit.

### **1.1.1 Motivation & Scope**

Traditional electromechanical accelerometers are being produced and used to fulfill navigation requirements by national defense organizations. But for applications like UAV's where weight is critical MEMS accelerometers are required. High performance MEMS accelerometers are under development and production internationally, but availability of such sensors is a matter of concern for our country. By designing such sensors we can indigenously fulfill our national needs.

UAV's are being produced at national level to meet defense requirements. To meet the navigation requirements for these applications high performance MEMS accelerometers are required.

## 1.2 Accelerometer Introduction

Accelerometer is a sensor used to detect and measure acceleration. In navigation systems this measured acceleration is integrated to estimate velocity and position displacement of navigating system. The principle of accelerometers is based on the measurement of the relative displacement that arises between the elastically suspended proof mass and the accelerometer frame subject to acceleration. This displacement of proof mass is due to inertia of proof mass. To attain a finite response time of the accelerometer a damped suspension of the proof-mass is used. Accelerations acting in the sensitive axis have the same effect like the static gravity. Mostly the accelerometer employs a capacitive pick-off system to detect displacement and this is used to command the feedback compensation.

The basic element of any accelerometer is a seismic mass which is suspended within a casing that is attached to a navigating object. The elastic structure (e.g., spring) that supports the mass and a displacement-sensing element are used to infer the force required to give the seismic mass the same motion as the test object.

Note that this is different from a displacement-type sensor that senses the relative motion between two points. Interestingly, a displacement-type sensing element is required inside most accelerometers to provide a measure of displacement or force, which can then be used to infer acceleration.

### 1.2.1 Performance Parameters

The basic performance parameters of any navigation grade accelerometers are its Resolution, Range, Scale Factor, Bias, Non linearity, Bandwidth, Temperature sensitivity and Short Term Stability to Long Term Repeatability of its performance parameters [1, 2]. These parameters are briefly defines as under,

Scale Factor- Output of accelerometer per unit input is called scale factor and defined in units of  $A/g$  ,  $V/g$ , pulses /g etc. where  $g$  is acceleration due to gravity.

Bias – Output of accelerometer without any input is called the bias and it is defined in units of ‘mg’ or  $\mu g$ .

Resolution- The minimum input acceleration that an accelerometer can detect with certain accuracy is defined as resolution of accelerometer and it is defined in units of ‘mg’ or  $\mu g$ .

Range-The maximum input acceleration that an accelerometer can detect is defined as

range in units of 'g'.

**Stability-** The standard deviation of output parameter (Scale factor, Bias) when operated over a specified period of time (minutes ~ few hours) in one run is defined as stability of that parameter.

**Repeatability-** The standard deviation of output parameter (Scale factor, Bias) when tested over a specified period of time (days, months, year) with intervals defined as repeatability of that parameter.

**Temperature Sensitivity-**the variation of parameter with change of temperature is defined as temperature sensitivity. It can be defined in units of ppm/°C for scale factor and mg or  $\mu\text{g}/^\circ\text{C}$  for bias of accelerometer.

Numerical limits of each of these performance parameters can define as per the navigation accuracy requirement of applications.

### **1.3 MEMS Accelerometers**

MEMS accelerometers are smaller as compared to the traditional high accuracy electromechanical accelerometers being used for navigation. Their smaller size is due to the fabrication technology used for fabrication of microelectronics. Accelerometers usually consist of a suspension system and a proof mass whose deflection provides a measure of the acceleration. There are different categories of MEMS accelerometers. This classification can be due to performance parameters or by their fabrication process or by the type of transduction mechanism used for detection of deflection of the proof mass of sensor.

Two types of fabrication methods are being used for fabrication of MEMS accelerometers. One method is of surface-micromachining which is suitable for integrating control electronics and mechanical structure in a single chip. This is mainly an additive process in which thin films of poly-silicon and silicon-oxide are grown on a wafer. The oxide layers act as sacrificial layers and can be removed by wet-etchant processes. The devices fabricated by this method are smaller than the devices fabricated by bulk-micromachining. Also this technology is compatible with a standard CMOS process and has led to monolithically integrated devices.

The other method is of bulk fabrication or material removal method. This uses the full

thickness of a wafer and is a subtractive process. Silicon is removed by wet or dry-etching techniques and forms a proof mass and a suspension system. These sensors may consist of a sandwich of multiple wafers bonded together to provide electrical contact an enclosure for the proof mass. Then this structure can be used with separate integrated circuit in the same package or even with discrete electronics but method is not suitable for monolithic integration. Therefore size of these devices can be larger than surface micro machined devices [3].

Also MEMS accelerometers are classified by types of transduction mechanisms used for detection of either force due to acceleration or deflection of the proof mass by the effect of acceleration. Different transduction methods are discussed separately.

### **1.3.1 Transduction Mechanisms**

A variety of transduction mechanisms have been used in MEMS accelerometers. Following is a list of few methods being used in accelerometers.

- a. Piezo-resistive
- b. Piezo-electric
- c. Capacitive
- d. Tunneling current
- e. Optical
- f. Thermal
- g. Resonant
- h. Magnetic

Each method of transduction has some advantages and unavoidable disadvantages [4-5]. A brief description of different transduction methods is described below.

Development of MEMS accelerometers was started using piezo-resistors technique. This method used piezo-resistive materials and fabrication of MEMS accelerometer using these materials was considered as an easy method and also a simple readout circuit was required. But these type of accelerometers had some problems as sensitivity of piezo-resistive MEMS accelerometers was low. Also temperature dependency of such accelerometers was high as compared to the capacitive sensors. Therefore, these are not preferred for high performance applications [6].



Another method used for fabrication of accelerometers was piezoelectric sensing method. Some materials produce charge under stress and in accelerometers stress is produced due to input acceleration. The sensitive material stores a charge on itself proportional to this external stress. Charge storage capability of the piezoelectric sensors makes them active devices, theoretically providing them to generate their own power and provides low power sensor design. Fabrication of piezoelectric sensors is also an easy method. By this method low cost sensor can be easily produced. But these types of accelerometers do not have a DC response. Also low frequency operation as required for navigation purpose is not feasible in this method [7].

Also a thermal method of acceleration measurement was used and in such accelerometers hot air bubble was used as a sensor proof mass, two thermal sensing electrodes were used for temperature difference detection. In balanced condition temperature difference of electrodes is zero while in input condition the air bubble can move and electrodes temperature changes. By this the acceleration is converted into temperature difference. This temperature difference is sensed and acceleration is measured [8]

Also tunneling current method is used for MES accelerometers fabrication. Such accelerometers are very sensitive and have higher bandwidth. Tunneling current occurs between two conductive layers that are located very close to each other. The distance between these electrodes should be about  $10 \text{ \AA}$  to create a tunneling current. By input acceleration the distance reduces and the tunneling current changes [9]. The advantage of such accelerometers is that a very low noise levels could be achieved. High drift values and fabrication complexity resulting in high cost of such accelerometers; this is the main disadvantages of these accelerometers.

Optical inertial sensors show high performances. The major advantages for optical inertial sensors are that they are immune to electromagnetic interference and they can operate at high temperatures. They show high performances but fabrication of light emitting and sensing components using micromachining techniques is complex and difficult [10].

In capacitive accelerometers proof mass displacement is detected with the change in the capacitance between the capacitive plates fabricated on each side of the proof mass. Capacitive based sensing gives greater design flexibility than piezoelectric quartz technology [6]. The capacitive devices are very popular for their high precision.

The widely and latest used techniques of MEMS accelerometers are the capacitive

sensing technique, as it is much appropriate for fabrication of MEMS. Capacitive sensors have multiple advantages when compared to the other types of accelerometers. Construction of capacitive accelerometers is very simple and this makes the fabrication cost low. Also power consumption of these sensors is low, have high sensitivity, high reliability as well as good nonlinearity, have low temperature dependency, have low noise, and low drift. These types are being preferred in consumer applications for their high performance, reliability, and low cost. Capacitive interfaces have several attractive features. In most micromachining technologies no or minimal additional processing is needed. Capacitors can operate sensors and actuators. Sensitivity over temperature is good when compared with other types. [11].

### **1.3.2 MEMS Accelerometers History**

A variety of MEMS accelerometer devices have been reported during last two decades. A brief history of some important devices is presented here.

Accelerometer with  $\pm 5g$  range was presented by H. Seidel et al. in 1990. The device was symmetrical differential with claimed minimum resolution acceleration value of  $1mg$  [12]. In 1991 E. Peeters et al. presented a device which was Helium filled to increase damping and stability of the device. The claimed measurement range of device was  $\pm 50g$  with  $80dB$  dynamic range [13]. Later on accelerometers were fabricated using DRIE processes. One such device was reported in 1997 by B.P. van Driee Nhuizen et al. A second order sigma-delta closed loop readout architecture was used in this device. Full scale range of  $5g$  was claimed by this team [14]. In the same year N. Yazdi and K. Najafi presented an accelerometer structure to achieve  $\mu g$  resolutions. In this study the mass was increased to decrease the mechanical noise. Also holes were fabricated in proof mass to decrease damping. The device mechanical structure design is shown in figure1.1. Although their aim was to achieve high resolution structures, but the results were not presented in their study [15].

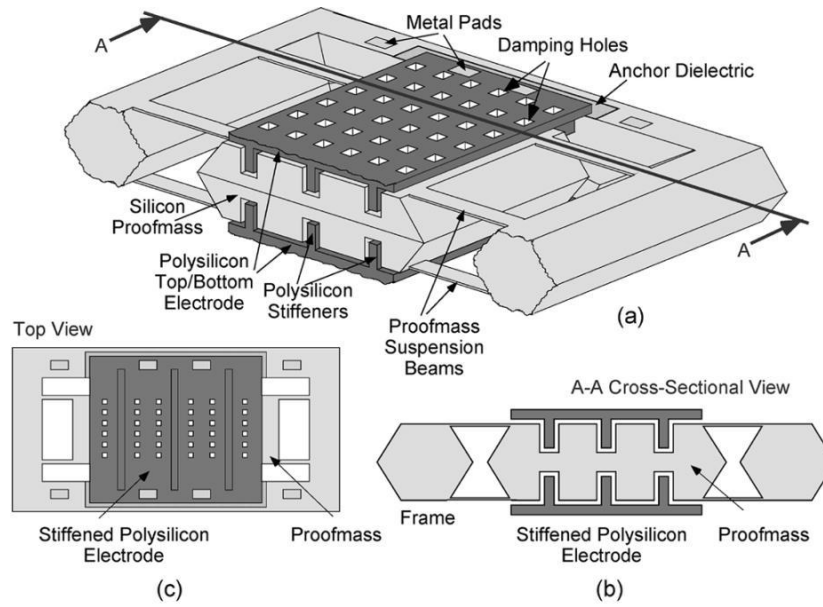
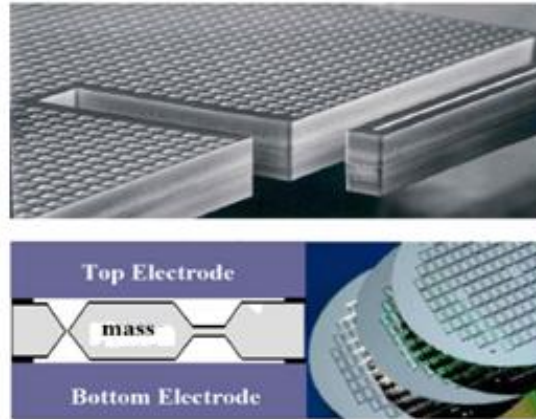


**Figure 1.1:** Mechanical structure design of the vertical axis accelerometer [15].

In 2003, self-balanced navigation-grade capacitive micro accelerometers was presented by Ki-Ho Han. The tests showed that the operating range is within  $\pm 2g$  [16].

In 2010, a leading MEMS inertial sensors company Colibrys, presented their commercial navigation grade accelerometer. This sensor operates in closed loop mode with second order sigma-delta multi-bit and high order 1-bit sigma-delta modulators. The accelerometer is fabricated through bulk micromachining with anisotropic etching of silicon to increase the yield and repeatability of manufacturing. Their sensor has a maximum measurement bandwidth of 400Hz and its bias instability is claimed as  $100\mu g$  [17]. A general view of structure of Colibrys accelerometer is presented in fig 1.2.

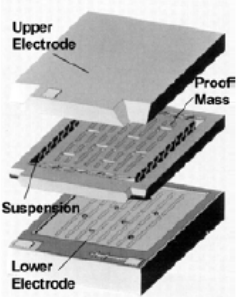
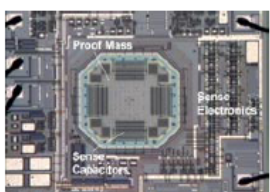
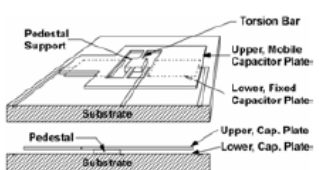
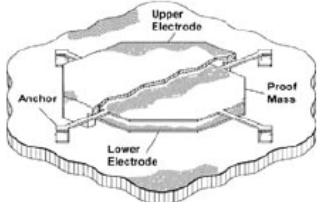
Also different companies have produced MEMS accelerometers for navigation and other applications. Different types of MEMS accelerometers devices are off the shelf available. Performance comparison of few commercial off the shelf available devices is presented by C. Acar and A M Shkel [4]. Design comparison of these devices is shown in figure 1.3.



**Figure 1.2:** Structure of out of plane capacitive MEMS accelerometer by Colibrys [17]

C Acar and A M Shkel

**Table 1.** Comparison of the properties of the evaluated sensors.

Endevco 7290A-10	Analog Devices ADXL210A	Silicon Designs SD2012-10	Motorola M1220D
 <ul style="list-style-type: none"> <li>● Out-of-plane</li> <li>● Bulk-micromachining</li> <li>● Two-chip</li> <li>● Single-crystal silicon</li> </ul>	 <ul style="list-style-type: none"> <li>● In-plane</li> <li>● Surface-micromachining</li> <li>● Integrated electronics</li> <li>● Polysilicon</li> </ul>	 <ul style="list-style-type: none"> <li>● Torsional</li> <li>● Electroforming</li> <li>● Two-chip</li> <li>● Nickel</li> </ul>	 <ul style="list-style-type: none"> <li>● Out-of-plane</li> <li>● Surface-micromachining</li> <li>● 'Cap' chip</li> <li>● Polysilicon</li> </ul>

**Figure 1.3:** Comparison of few commercial MEMS accelerometers [4].

## 1.4 Navigation Grade Accelerometer

Accelerometers are the important sensors of inertial navigation systems. Traditional high accuracy electromechanical accelerometers with quartz pendulum are highly accurate with resolution of  $<1\mu\text{g}$  and one year repeatability of  $\leq 50 \mu\text{g}$  with input range of  $\pm 50 \text{ g}$  but also are very expensive [1]. Whereas the best available MEMS devices with input range of  $\pm 10\text{g}$  have resolution of up to  $250 \mu\text{g}$  and max repeatability of  $25\text{mg}$  [2] but cost of MEMS sensors is very low as compared to traditional electromechanical accelerometers. Although accuracy of MEMS

accelerometers is yet not comparable to quartz flexure accelerometers but due to their mass production process these provide very economical solution particularly for low accuracy navigation applications. MEMS accelerometers are widely being used in automobiles but their accuracy is not enough for high accuracy inertial navigation use. Variety of MEMS accelerometers are being developed and reported for navigation applications. Most of these are capacitive devices with electrostatic rebalancing mechanisms. Recently reported ultra precision MEMS accelerometer developed by Colibrys is also a capacitive device working in close loop based on electro static rebalancing [17-18].

Typical performance parameters of accelerometers with medium resolution for automotive applications and high performance for inertial navigation applications are presented by [6] as shown in table1.1 below. Also Figure 1.2 shows the acceleration-bandwidth performance requirements of different application areas for accelerometers [3].

**Table 1-1:** Typical specifications of accelerometers for automotive and inertial navigation applications [6]

<b>Parameters</b>	<b>Automotive</b>	<b>Navigation</b>
Range	$\pm 50$ g (air bag) $\pm 2$ g (vehicle stability System)	$\pm 1$ g
Frequency Range	DC- 400 Hz	DC- 100 Hz
Resolution	$< 100$ mg (air bag) $< 10$ mg (vehicle stability System)	$< 4\mu$ g
Off-axis sensitivity	$< 5\%$	$< 0.1\%$
Nonlinearity	$< 2\%$	$< 0.1\%$
Max. Shock in 1msec	$> 2000$ g	$> 10$ g
Temp Rang	$-40^{\circ}\text{C}$ to $85^{\circ}\text{C}$	$-40^{\circ}\text{C}$ to $80^{\circ}\text{C}$
TC of offset	$< 60$ mg/ $^{\circ}\text{C}$	$< 50\mu$ g/ $^{\circ}\text{C}$
TC of Sensitivity	$< 900$ ppm/ $^{\circ}\text{C}$	$\pm 50$ ppm/ $^{\circ}\text{C}$

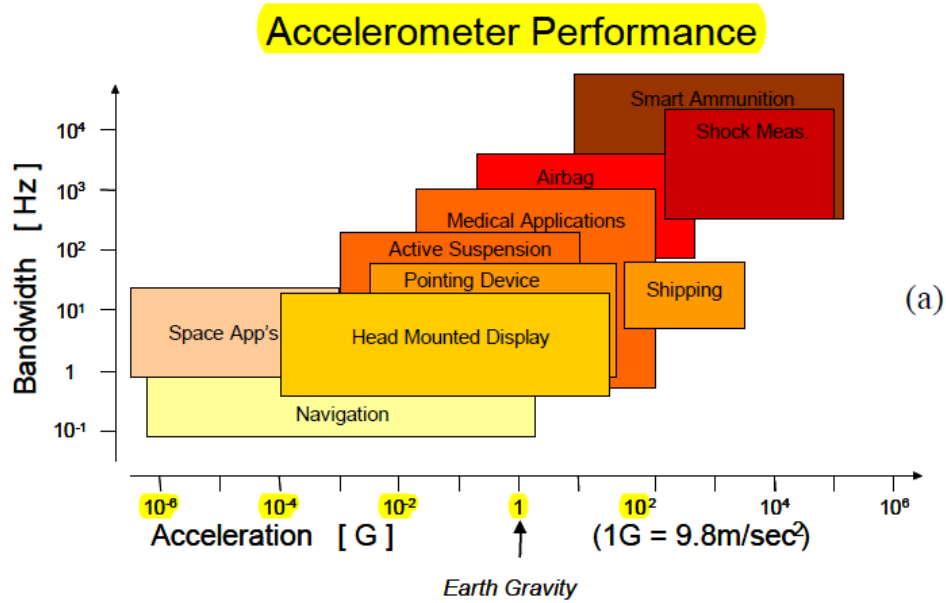


**Figure 1.4:** Accelerometer performance requirement for different applications [3]

Performance requirements for any application may depend upon the required accuracy of navigation, duration of navigation or the environment of application. Accelerometer performance can be characterized with two parameters: scale factor & bias stability [19]. It may be concluded that accelerometer for navigation should have lowest value of resolution, bandwidth of 100 Hz and range of 10 g is sufficient for convention applications of navigation.

Therefore the performance parameters set as a reference of this research work accelerometer are listed in table below.

**Table 1-2:** Target performance parameters for navigation grade accelerometer

Sr.#	Parameters	Navigation
1	Range	$\pm 10$ g
2	Frequency Range	DC - 100 Hz
3	Resolution	$\leq 10$ $\mu$ g

## CHAPTER 2: MAGNETS IN MEMS

Permanent magnets are being used in micro-systems such as micro-actuators and MEMS energy harvesters. Magnetic micro-electromechanical systems (MEMS) present new class of micro-scale devices that incorporate magnetic materials as sensing or active elements. The introduction of magnetic MEMS has prompted a whole new range of applications. One of the new areas of applications is micro-actuators. Though electrostatic micro-actuators have dominated the field owing to some obvious advantages like ease of integration in microelectronic systems and better force scaling, in recent years there has seen an increased interest in magnetic micro-actuators. The trend is driven by the unique capabilities of magnetic systems, such as wireless and bidirectional control and significantly larger actuation displacements.

Since MEMS have evolved from the microelectronics industry, electrostatic interactions have been advantaged from the very beginning as the primary actuation mechanism in these systems. Also use of electrostatic force is very common in microelectronic systems due to its better force scaling at micro scale level and also technology is highly developed as compared to electromagnetic systems at micro level[20]. Scaling differences of electrostatic and electromagnetic forces is discussed in details by Edward P Furlani [21]. Magnetic field from electromagnet unfavorably scales with diminishing sizing, whereas the fields from permanent magnet are scale invariant. Source of magnetic field in electromagnet is current but the magnetic field in permanent magnet is residual magnetization which arises at atomic level [21]. For actuation electromagnetic force is more stable for high force and for large gaps [22].

### 2.1 Magnetics Materials

The materials that have their own magnetic field or they help to improve magnetic field are known as magnetic materials. Depending on the coercivity of materials these materials are further classified as soft magnetic materials and hard magnetic materials.

#### 2.1.1 Hard Magnets

Permanent magnets are the materials that exhibit magnetization in the absence of external magnetic field as once these materials are magnetized they retain their field. These materials have high coercivity so these materials are difficult to magnetize and demagnetize. Coercivity

and romance are the important properties in the selection of magnet for any application. The common hard magnetic materials are ferrites, alnico, samarium cobalt, neodymium iron boron etc.

Permanent magnets are used for the development of high performance micro magnetic systems like energy harvesters, generators, motors, switches and acoustic speakers etc.

### **2.1.2 Soft Magnets**

Soft magnets are those materials that do not retain their magnetization and are quickly demagnetized when applied magnetic field is removed. These materials have low coercivity so these materials are quickly magnetized and demagnetized by application and removal of external magnetic field. But permeability of these materials is very high therefore these materials increase the magnetic field or confine or focus the magnetic flux of external field. Soft magnets are often coupled with permanent magnets as a core to guide and concentrate magnetic field in specific regions e.g, across coils for an electromagnetic actuator. The common soft magnetic materials are soft iron, and nickel-iron alloys.

## **2.2 Challenges for use of Hard Magnets in MEMS**

Unlike soft magnetic films there is no preexisting knowledge base from which to draw the need of relatively thick film of hard magnetic materials is somewhat unique to MEMS applications.

- The magnetic performance, temperature effects, chemical stability and fabrication constraints all play role in the material selection and micro fabrication strategy.
- The material properties of most hard magnets are typically quite sensitive to both the microstructure and the chemical composition. This requires careful control over the processing conditions and may require the application of magnetic field, additional thermal steps or the processing steps to optimal magnetic properties thus adding cost and complexity to the fabrication.
- Hard magnets require in situ or post fabrication magnetization steps to pole the magnets in a specific direction, this complicates the integration process, particularly for wafer



scale batch fabrication. It also implies that all magnets on a wafer are magnetized in only one direction, which restricts the device design.

- Perhaps most importantly the total system performance of a magnet based system usually limited by the magnet. Thus quality and performance of the magnetic material plays a critical role in the overall design.

### **2.2.1 Fabrication of Magnets in MEMS**

At macro scale powder metallurgy is used to fabricate permanent magnets as per required shape and size. In this technique the magnetic powder is mechanically pressed and then heat treated to form dense/ sintered magnets with strong magnetic properties. Also in some cases magnetic powder can be combined with polymers resin to fabricate less brittle magnets.

Limitations for MEMS Fabrication:

Use of magnets in MEMS devices is increasing but for MEMS applications the method of powder metallurgy sintering has few limitations.

- Powder metallurgy sintering method is not well suited for very small magnet sizes of less than 1mm and for high accuracy requirements like as required in MEMS.
- Assembly of separately fabricated magnets in MEMS fabrication batch increases manufacturing complexity and cost especially if precise positioning or multiple magnets are required.

Earlier methods like bottom up micro fabrication deposition approaches were used as the integration of permanent magnets materials in MEMS, traditional thin film deposition method like physical vapor deposition technique as sputtering and pulse laser deposition and electrochemical processes such as electroplating were used for fabrication of magnets in MEMS.

These techniques have very slow deposition rates, sensitivity to processing conditions and often the requirement of high temperature annealing in order to realize strong magnetic properties. This fabrication of thick (ten to hundreds of micrometer) high quality magnetic layer becomes complicated, expensive time prohibitive or process incompatible.

### **2.3 Future of Magnets in MEMS**

Use of permanent magnets was limited in MEMS due to difficulties of their fabrication at micro scale level but now it is increasing as different fabrication technologies are being reported. Larger actuation distance can be achieved by using magnets as compared to electrostatic actuation [21, 23, and 24]. Magnetic actuators can be more favorable than electrostatic actuators when the actuation gap is greater than  $2\ \mu\text{m}$  but this requires a thick structure of magnetic material.

Unconventional strategies of using magnetic powders of 5~50 micrometer sizes are being adopted to fabricate magnets of required size at wafer levels. Details and performance of this method is discussed in details by Ololade D Oniku [23].

Permanent magnet is used in traditional navigation grade electromechanical accelerometers. In MEMS accelerometer to get  $\mu\text{g}$  resolution and low noise of accelerometer a heavier proof mass is recommended and to rebalance this proof mass an electromagnetic system with a permanent magnet can be used. Permanent magnets fabrication using magnetic powder and fabrication at wafer level can be adopted for this design. Doctor's blade technique as discussed in ref [23] can be easily adopted at wafer fabrication for this design. Details of the method are discussed in fabrication chapter.

## CHAPTER 3: ANALYTICAL MODEL AND PROPOSED DESIGN

Basic working principle of an accelerometer with an analytical model is described in this chapter. A permanent magnet based MEMS accelerometer design is proposed and its complete functioning is described.

### 3.1 Analytical Model of Accelerometer Working Principle

A basic model of an accelerometer can be defined as second order mass spring-damper system as shown in figure 3.1. Where ‘m’ is the mass of the moving body, ‘b’ is air damping coefficient, ‘k’ is the stiffness or the spring constants, ‘x’ is the displacement of mass and ‘a’ is the input applied acceleration of the system. Mathematically this can be expressed as

$$F = ma = m\ddot{x} + b\dot{x} + kx \quad \text{--- 1}$$

Transfer function of this system for deflection of mass can be defined as

$$H(s) = \frac{x(s)}{a(s)} = \frac{1}{s^2 + \frac{b}{m}s + \frac{k}{m}} \quad \text{--- 2}$$

Using this second order equation the natural resonance frequency and quality factor of this basic accelerometer can be calculated

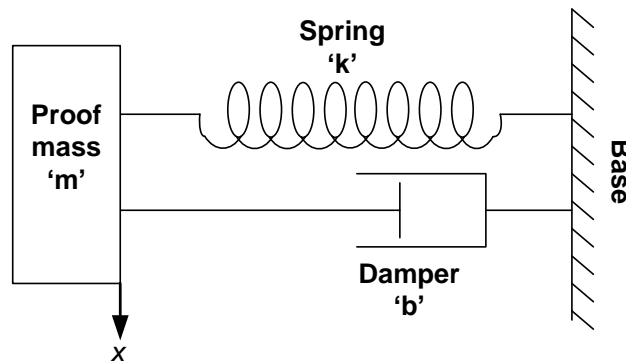


**Figure 3.1:** Accelerometer working principle

Natural frequency of system,  $w_o = \sqrt{\frac{k}{m}} \quad \text{--- 3}$

Quality factor,  $Q = \sqrt{\frac{km}{b}} \quad \text{--- 4}$

Also the static response of this system can be defines as

$$\frac{x-static}{a} = \frac{m}{k} = \frac{1}{w_o^2} \quad \text{--- 5}$$

From these equations it can be seen that static response of the system can be increased by reducing the system natural frequency and this natural frequency can be reduced by increasing mass and reducing spring constant of spring. This is a basic model for an accelerometer when operated in an open loop system but when a closed loop is applied then this system can be modeled as shown in figure 3.2.

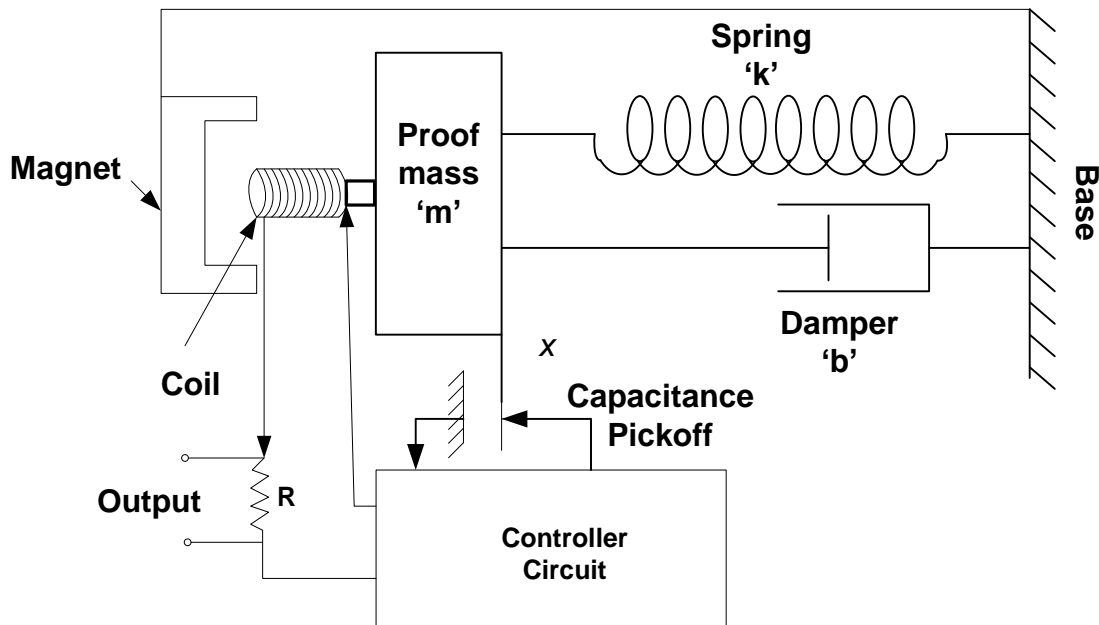


**Figure 3.2:** Close loop accelerometer working principle

The applied acceleration  $a$  produces inertia force  $F = ma$  on the mass  $m$ . And this force is balanced by the force of the permanent magnet on the current carrying coil (rebalance or feedback coil). Any imbalance of these two opposite forces results in the displacement of mass from centre position which is detected by the displacement sensor like potentiometer, capacitive pick off or any suitable method. This pickoff signal is amplified in a controller producing a current output that is fed to the feedback/ rebalance coil. A resistor is used to get a voltage output of complete system. A block diagram of complete system is shown in figure 3.3.

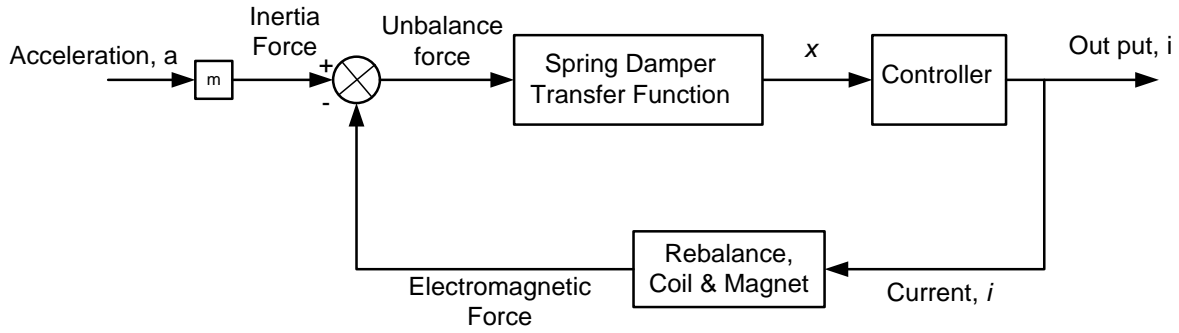


**Figure 3.3:** Block diagram of close loop system

This block diagram of system consists of three transfer functions; the spring damper transfer function is already explained while the controller transfer function and gain of controller are designed as per overall frequency performance requirement of system. This controller block can be divided in to further separate block of pickoff system and amplifier blocks. By selecting suitable controller parameters the natural frequency of the system can be achieved much higher than the frequency of open loop mass spring system.

### 3.2 Proposed Design Outline

A permanent magnet based MEMS accelerometer design is proposed and analyzed. It is a three wafer design in which the centre wafer with proof mass is sandwiched between two symmetrical permanent magnet wafers as shown in figure 3.4. The bench mark of the design is to use permanent magnet for rebalancing of proof mass of MEMS sensor instead of electrostatic rebalancing. Permanent magnet with volume of  $0.5\text{mm}^3$  has been selected to get bulk fabrication with powder size of  $5\sim 50\ \mu\text{m}$  and this can be accommodated in  $500\ \mu\text{m}$  thick wafer. Proof mass includes the rebalance coils and capacitance area for pickoffs as shown in figure 3.4-a. The designed proof mass has total area of  $18\ \text{mm}^2$  ( $18\text{e}6\ \mu\text{m}^2$ ) with thickness of  $500\ \mu\text{m}$  and coils mass is additional. This heavy proof mass results in a low Brownian noise [26] and greater stability and repeatability. The proof mass is suspended by two flexure beams attached to the fixed frame of centre wafer. In response to the applied input acceleration the proof mass deflects and change in capacitance is detected. One side capacitance area for pickoff is  $11\ \text{mm}^2$  which is large as compared to in plane MEMS accelerometers, this result in fine pickoff resolution. Rebalance force is applied by the passing current through the coils present on the proof mass.

This current is the output of the accelerometer giving information about the acceleration applied to the system.

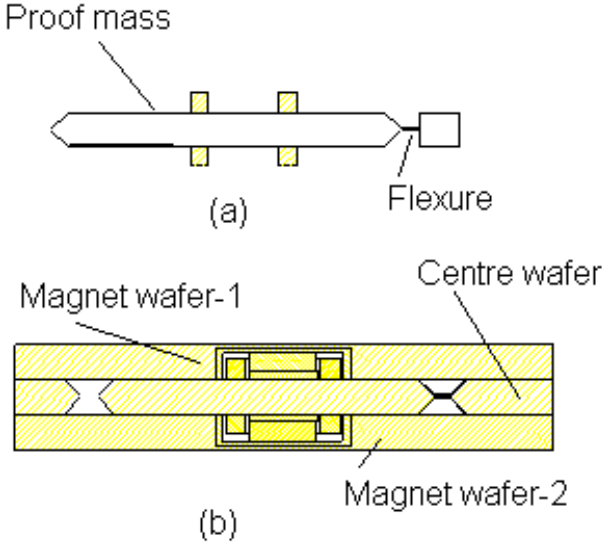


**Figure 3.4:** Three wafer design diagram

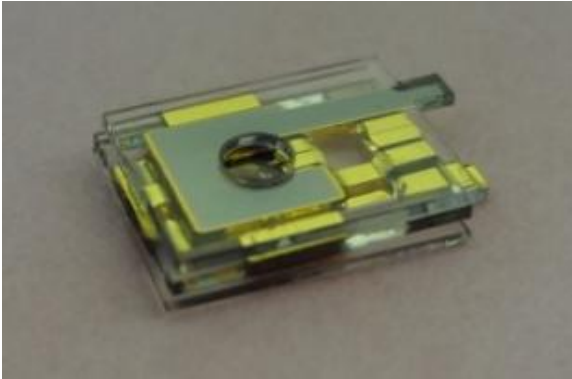


**Figure 3.5:** Three wafer fabricated device (without coils & magnet)

For an applied input acceleration the total force depends on the total proof mass of pendulum part. This input force is to be balanced by coils. Lorentz force of the coils with current flowing through is the rebalance force. The Lorentz force on a conductor of length ‘L’ and with the current ‘i’ in an externally generated magnetic flux density ‘B’ perpendicular to the wire is

given by  $F = Li \times B$ . Rebalance force is directly proportional to the magnetic field available in the working gap of coil. To get maximum force magnetic field and coil placement need to be optimized. To get maximum magnetic field in working gap of coil a magnetic loop is designed. Also to get maximum force, magnetic field direction should be perpendicular to the current flowing through the coil. Different configurations of magnetic system with permanent magnet and soft magnet materials are proposed, performance of each is evaluated to select the best possible configuration. Field variation in two dimensions is simulated during analysis of system to get optimized location of coil. Variation of flux density along z direction is also studied.

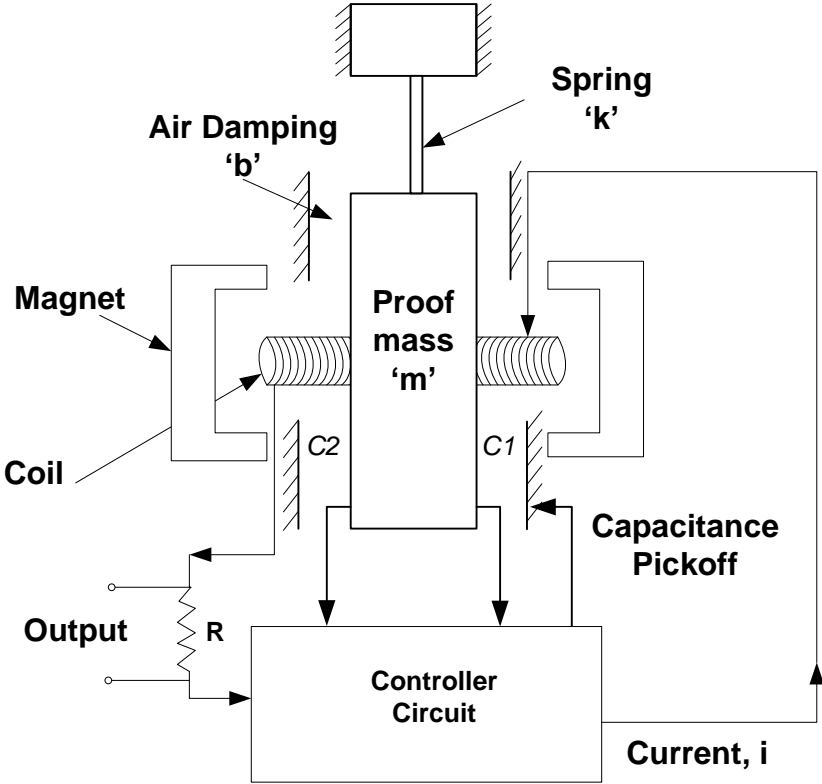


**Figure 3.6:** Analytical model of proposed design

## CHAPTER 4: MODELING OF DESIGN PARAMETERS

The design and functioning of accelerometer is discussed in previous chapter. Parameters required for the complete analytical model of accelerometer are designed, calculated or estimated in this chapter. The model parameters of the designed accelerometer can be divided into two parts. Part one covers the parameters related to the structure and part two covers the parameters related to the pick off and control system of the design.

The structure part consists of three wafers and of these three wafer two wafers acts as fix structure while the third wafer sandwiched between two wafers acts as a sensor to detect acceleration due to inertia. The dynamic part of this of accelerometer design is only the centre wafer part. Main features of this part are the two flexures, capacitive surface, rebalance coils, proof mass of pendulum part and the damping coefficient of the dynamic proof mass. A model of these three wafers is shown in figure 4.1 below.

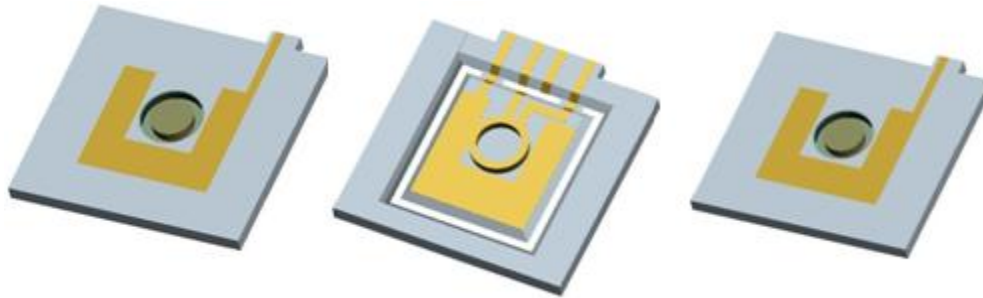


**Figure 4.1:** Three wafer design model

### 4.1 Parameter Estimation of Flexure Part

The basic parameters required for the analytical model of proposed design are designed, calculated and estimated below. These parameters include spring stiffness, mass and moment of inertia of the proof mass and the damping coefficient estimation.

#### 4.1.1 Spring Constant / Stiffness of Hinge Estimation:

In accelerometers spring constant of the hinge is very important for the performances of the sensors. The performance of the sensor is related with the easiness in the movement of the proof mass in the sensitive axis and also with the difficulty in the movement of the proof mass in the other axes. Hence, determining the spring constants in all directions is an important design



step. The stiffness in the input axis is most important for resolution of the sensor. Input axis stiffness should be lowest to detect the smallest input acceleration but at the same time this flexure spring should be strong enough to resist breakage during manufacturing, assembling, operation and non operation duration. The stiffness depends on the dimension of flexure hinges and material elasticity. Initially dimension of flexure length, width and thickness are supposed and then by iteration process these values are finalized get stiffness and strength of flexures.

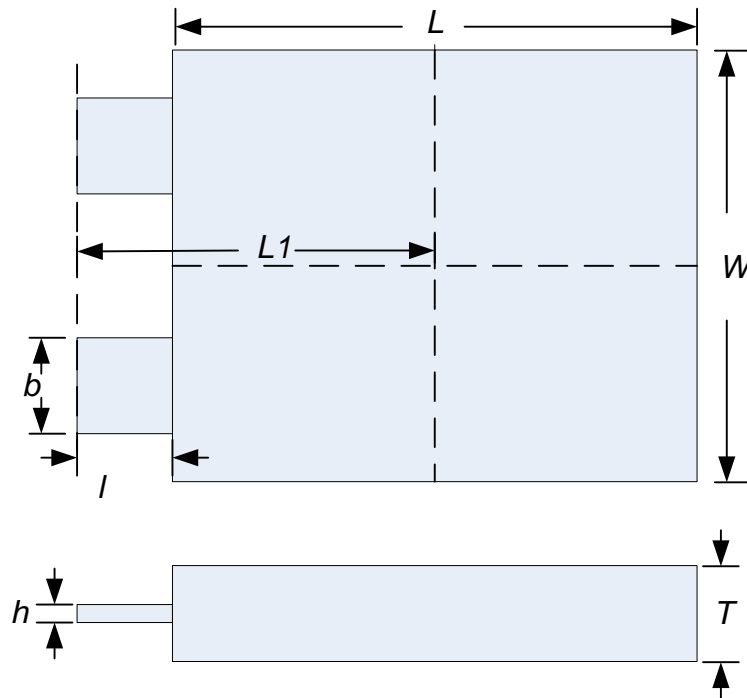


**Figure 4.2:** Design parameter dimensions

**Table 4-1:** Design parameters dimension values

Sr. #	Parameter	Value	Units
1	Width of flexure hinge, $b$	700	$\mu\text{m}$
2	Thickness of flexure hinge, $h$	8	$\mu\text{m}$
3	Length of flexure hinge, $l$	800	$\mu\text{m}$
4	Length of rigid part, $L$	4500	$\mu\text{m}$
5	Width of rigid part, $W$	4000	$\mu\text{m}$
6	Thickness of wafer, $T$	500	$\mu\text{m}$

Stiffness of flexure can be calculated using equation 6 as under.

$$\text{Stiffness of flexure, } k = \frac{Ej}{l} \quad \text{--- 6}$$

Where

$$E - \text{Modulus of elasticity of Fused Silica (quartz)} = 7.3 \times 10^6 \text{ g/mm}^2$$

$J$  – Area Moment

$l$  – Length of flexure

$$\text{Area moment of flexure is calculated as } J = b.h^3/12 \quad \text{--- 7}$$

$$J = \{0.7 \times (0.008)^3\}/12 = 2.98 \times 10^{-8} \text{ mm}^4$$

Substituting values in equation 6, the stiffness of one flexure hinge is calculated as

$$k_1 = \frac{Ej}{l} = (7.3 \times 10^6 \times 2.98 \times 10^{-8})/0.80 \text{ (g/mm}^2 \cdot \text{mm}^4/\text{mm)}$$

$$= 0.273 \text{ g.mm/ rad.}$$

Total stiffness of two flexure hinges is calculated as under

$$k = k_1 + k_2 = 2 \times k_1 \quad \text{as } k_1 = k_2 \text{ both flexures are same}$$

$$k = 2 \times 0.273 = 0.546 \text{ g. mm / rad.}$$

#### 4.1.2 Moment of Inertia Calculation:

Moment of inertia of this structure can be estimated using equation ‘8’ as stated below.

$$J = \frac{V \rho L^2}{g} \quad \text{--- 8}$$

Where,  $V$  = Volume of proof mass part

$\rho$  = Material density

$L_I$  = Distance from centre of gravity to axis of rotation

As the total proof mass consists of two parts, one is the wafer substrate and second is the rebalance coils fabricated over the substrate. Inertia values are calculated separately and then added to calculate the total inertia of proof mass.

First part is wafer substrate

$$V = L \times W \times T = 4500 \times 4000 \times 500 = 9E+9 \mu \text{ m}^3 = 9 \text{ mm}^3$$

$$\rho = 0.00233 \text{ g/mm}^3, \quad L_I = 3 \text{ mm} \quad g = 9.81 \text{ m/s}^2$$

$$J_1 = (9) \times (0.00233) \times (3)^2 / 9.81 \text{ e}3 = 1.92 \text{ E-}05 \text{ g-mm-s}^2$$

Second part is rebalance coils, Total volume of two coils is  $V_c = 11.88 \text{ mm}^3$ , coil material is copper with density  $\rho = 0.009 \text{ g/mm}^3$ , and moment arm length is  $L_1 = 3 \text{ mm}$  moment is calculated as

$$J_2 = 0.644 \times 0.009 \times (3)^2 / 9.81 \times 10^3 = 0.00000532 \text{ g-mm-s}^2$$

Total moment of the proof mass is calculated by adding two calculated values

$$J = J_1 + J_2 = 0.00002452 \text{ g-mm-s}^2$$

### 4.1.3 Damping Coefficient Estimation:

Damping coefficient includes the energy dissipative effects during the operation of a micromechanical device. These effects may be the viscous air damping, structural material losses, energy loss through the anchors, etc. At atmospheric pressure, viscous air damping is the dominant dissipative process.

The motion of a typical lateral accelerometer is in the direction parallel to the substrate surface. The major damping mechanism for a laterally moving accelerometer operating under the atmospheric pressure is the squeeze film damping between the capacitive areas. There are also other minor damping mechanisms like slide film damping which can be neglected compared with the squeeze film damping for a micro machined lateral accelerometer. In squeeze-film damping, the motion of the mass is in such a way that the air molecules between the mass and the substrate are squeezed and they try to escape from the decreasing volume under the mass. Damping coefficient is estimated here as follows.

a- For annular plate

$$b = \frac{3 \mu R^2 A}{2h^3} G(\beta) \quad \text{--- 9}$$

$$\text{Where } G(\beta) = 1 - \beta^4 + \frac{(1 - \beta^2)^2}{\ln(\beta)} \quad \text{--- 10}$$

$$\beta = r/R$$

R = radius of plate

r = radius of hole in plate

Plate is square but equivalent radius 'R' can be calculated from area of plate

$$\text{Surface area} = 4 \times 4.5 = 18 \text{ mm}^2$$

$$\text{Equivalent radius } R = \sqrt{\frac{18}{\pi}} = 2.394 \text{ mm (for circle Area} = \pi R^2)$$

Radius of hole,  $r = 1 \text{ mm}$ ;  
 $\beta = r/R = 1/2.394 = 0.4177$ ;  $G(\beta) = 0.1888$

$b = 0.1027 \text{ g-s/mm}$

For angular damping the moment of damping coefficient is calculated as below.

$b = 0.1027 \times (3)^2 = 0.9244 \text{ g-s-mm}$

## 4.2 Close loop System Model & Parameters Estimation

In this part the parameters related to the pickoff and control system are estimated. The complete close loop working of system is presented in a block diagram in figure 4.3 shown below. The parameters for the transfer function of  $G_p$  are calculated earlier. Here the parameters for the pickoff and control system are estimated to complete the functioning of accelerometer system. The structure mass spring system is modeled as a pendulum system therefore the result of input to the pendulum is an angle ' $\alpha$ ', this angle is converted into a capacitance change, then this change of capacitance is converted into a voltage change and this voltage change is amplified into a current, this current is then fed to the feedback coils to rebalance the input inertia force. Gains of all these blocks are calculated to estimate a stable feedback system.

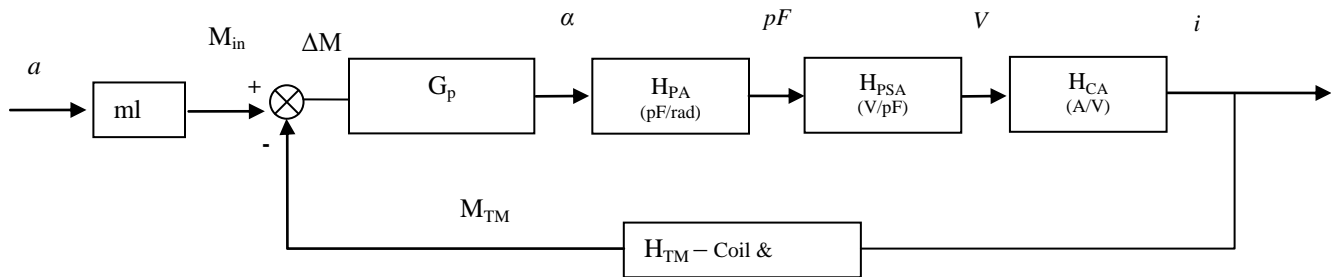


**Figure 4.3:** Complete system model

$$J \cdot \ddot{\alpha} + b \cdot \dot{\alpha} + k \cdot \alpha = M_{in} - M_{TM} \quad \text{--- 11}$$

$$J \cdot \ddot{\alpha} + b \cdot \dot{\alpha} + k \cdot \alpha = \Delta M \quad \text{--- 12}$$

$M_{in}$  – Deflection moment

$M_{TM}$  – Torquer Moment

$G_P$  - Transfer function of pendulum system

$H_{PA}$  – Pickoff Angular Sensor (pF/rad)

$H_{PSA}$  – Pickoff Sensor Amplifier (V/pF)

$H_{CA}$ – Control Amplifier (A/V)

$H_{TM}$  – Torque Moment, (g-mm/A)

At this stage overall gain of this close loop system must be determined as this depends on the minimum target input required to be detected. The minimum input will produce a smallest deflection and this deflection must be detected by the pickoff system and consequently balanced by the close loop system. This minimum deflection is determined by the stiffness of hinges and is calculated as

Target minimum input (resolution) = 10 $\mu$ g

Torque by minimum input = 8.04E-7 g-mm (as for 1 g input it is  $ml = 0.08042$  g-mm)

Deflection by minimum input = input torque / stiffness = 8.04E-7 /0.54 rad  
= 1.38E-6 rad

Over all close loop system gain,  $K_{loop}$  = Pendulum moment / Minimum Deflection  
= (0.080425\*15)/1.38e-6 = 8.7E5 g-mm/rad

As a very small deflection is to be detected therefore a high gain is required for the close loop system. The overall close loop system is divided into different gain blocks. Total gain of these blocks should equal to the overall gain required for close loop system.

$$K_{loop} = K_{PA} \cdot K_{PSA} \cdot K_{CA} \cdot K_{TM} \quad \text{--- 13}$$

The gains of “ $K_{PA}$ ” and “ $K_{TM}$ ” are limited by the capacitance gap , area and the rebalance torque coils with magnet while the others will be designed to achieve overall close loop system gain. Gains and transfer function of each block are calculated separately as under.

#### 4.2.1 Pickoff Angle Sensor - $H_{PA}$ (pF/rad)

Gain of angular deflection sensing can be assumed as a linear relation as  $H_{PA}$  in pF/arc-sec or arc-min. Capacitance in nominal centre position is calculated as under equation 14,

$$C_{nom} = 8.85 \frac{S}{d} 10^{-12} \text{ F} \quad \text{--- 14}$$

Where  $S$  = surface area = 11 mm<sup>2</sup> or 11x10<sup>-6</sup> m<sup>2</sup>

$d = \text{capacitor distance} = 10 \times 10^{-2} \text{ mm or } 10 \times 10^{-6} \text{ m}$

$\epsilon = 1$

$C_{\text{nom}} = 9.735 \text{ pF}$

If pendulum is deflected 1 arc min then linear distance change is calculated as

1 arc-min =  $3 \times 10^{-4}$  rad

$$x = 3 \text{ mm} \times \sin(3 \times 10^{-4} \text{ rad}) = 3 \times 3 \times 10^{-4} = 9 \times 10^{-4} \text{ mm} = 0.9 \text{ } \mu\text{m}$$

Now calculate capacitance by change of this distance.

Capacitance for new distance after 1 arc-min deflection (10-0.9) i.e 9.1  $\mu\text{m}$

$$= 8.85 \epsilon \frac{S}{d} 10^{-12} \text{ F} = 10.7 \text{ pF}$$

Change in capacitance by deflection of 1 arc- min

$$\Delta C = 10.7 - 9.735 = 0.965 \text{ pF}$$

Differential capacitance for two capacitor sides

$$\sum \Delta C = 0.965 \text{ pF} \times 2 \approx 1.93 \text{ pF}$$

$$K_{\text{PA}} = 1.93 \text{ pF/arc-min} = 1.93 \times 60 \times 57.3 = 6635 \text{ pF/rad}$$

#### 4.2.2 Torquer Moment Transfer Function - HTM in g-mm/A

Transfer function of the torque coils as a first approximation can be assumed as direct relation. This value can be obtained by knowing the nominal value of the static moment of the pendulum and the current flowing through the coil.

Static moment of pendulum  $M_{\text{st}} = 0.0804 \text{ gram-mm}$

$I = 1 \text{ mA/g}$  assumed SF

0.0804 g-mm is balanced by 1 mA

So how much torque will be available by 1 A current is

0.0804 g-mm : 1 mA

$K_{\text{TM}}$  g-mm : 1000 mA

$$K_{\text{TM}} = 80.4 \text{ g-mm/A}$$

$$H_{\text{TM}} = K_{\text{TM}} / (\tau_{\text{TM}} s + 1) \quad \text{--- 15}$$

Where  $\tau_{\text{TM}} = \frac{L}{R}$

Coil Resistance and Inductance are estimated as under

X-section area of wire =  $20 \times 20 = 400 \mu\text{m}^2$

Equivalent radius =  $r = 11.2 \mu\text{m}$

Mean Diameter of coil =  $D = 1.55 \text{ mm}$

No. of turns =  $n = 144$

Total length of wire =  $\pi D n = 700 \text{ mm}$

Resistivity of the coil material  $\rho = 1.678 \text{E-}8 \text{ Ohm-m}$

Resistance,  $R = \rho l / a = 1.678 \text{E-}8 * 700.85 \text{E-}3 / 400 \text{E-}12 = 29.4 \text{ Ohm}$

$\mu_0 = 4 \pi \text{E-}3 \text{ Wm/A-m}$

Inductance of the coil ,  $L = \mu_0 n^2 A l = 1.6 \text{ mH}$

$\tau_{\text{TM}} = \frac{L}{R} = 1.6 \text{E-}3 / 29.4 = 5.4 \text{E-}5$

$$H_{\text{TM}} = K_{\text{TM}} / (\tau_{\text{TM}} s + 1) \quad \text{--- 16}$$

$$H_{\text{TM}} = \frac{80.4}{5.4 \text{e-}5 s + 1}$$

### 4.2.3 Pickoff Sensor Amplifier Transfer Function - $H_{\text{PSA}}$ in V/ pF & Control Amplifier - $H_{\text{CA}}$ in A/V

As the gains of “Pickoff Angle Sensor” and “Torquer Moment” are calculated, now the gain of Pickoff Sensor Amplifier & Control Amplifier can be calculated is calculated using equation 13,

$$\begin{aligned} K_{\text{CA}} \cdot K_{\text{PSA}} &= \frac{K_{\text{loop}}}{K_{\text{PA}} \cdot K_{\text{TM}}} \quad \text{--- 17} \\ &= (8.7 \text{E}5) / (6635 \times 84.4) \\ K_{\text{CA}} \cdot K_{\text{PSA}} &= 1.5 \end{aligned}$$

This is the gain required for the pickoff sensor and the controller amplifier. Let's suppose the gain of pick off sensor amplifier is  $K_{\text{PSA}} = 200 \text{ mV/pF} = 0.2 \text{V/pF}$  the gain of controller will be  $K_{\text{CA}} = 0.75$

For “Pickoff Sensor Amplifier Transfer Function” a signal is used to pickoff capacitance therefore a time constant is to be calculated. Transfer function of “Pick off Sensor Amplifier” is given as per equation 18

$$H_{\text{PSA}} = K_{\text{PSA}} / (\tau_{\text{PSA}} \cdot s + 1) \quad \text{--- 18}$$

Time constant of a pickoff capacitance can be assumed using the frequency of the pick off signal if there are no experimental data available. Here it is calculated formula a per equation 19

$$\tau_{PSA} = \frac{1}{\pi \cdot f} \quad \text{--- 19}$$

where f – frequency of an input signal used for capacitance pickoff

$$\tau_{PSA} = \frac{1}{\pi \cdot 50000} = 6.37e^{-6} \text{ sec}$$

$$\text{Thus } H_{PSA} = 0.2 / (6.37e^{-6} \text{ s} + 1) \quad \text{V/pF}$$

In this way all the close loop system model parameters are estimated, calculated and finalized.

Analysis of the complete system is carried out as given in analysis chapter.



## CHAPTER 5: DESIGN AND STRUCTURAL ANALYSIS

### 5.1 Structure Analysis

Structure analysis of the design is carried out to ensure its survival in its manufacturing and operation life. Both analytical and FEM methods are used to estimate stresses in the sensor part flexures.

#### 5.1.1 Analytical Structure Analysis

Sensor structure can be subjected to different forces during manufacturing, storage and operational life. Analysis of designed structure is carried out to evaluate its survival/performances in different conditions. Flexures are the critical parts that are under stress, in free condition when centre part is not fixed between two wafers the centre part can bend freely and subjected to maximum stress as shown in figure 4.1. Input moment is defined as 'M' where 'P' is the mass of proof mass part of centre wafer.

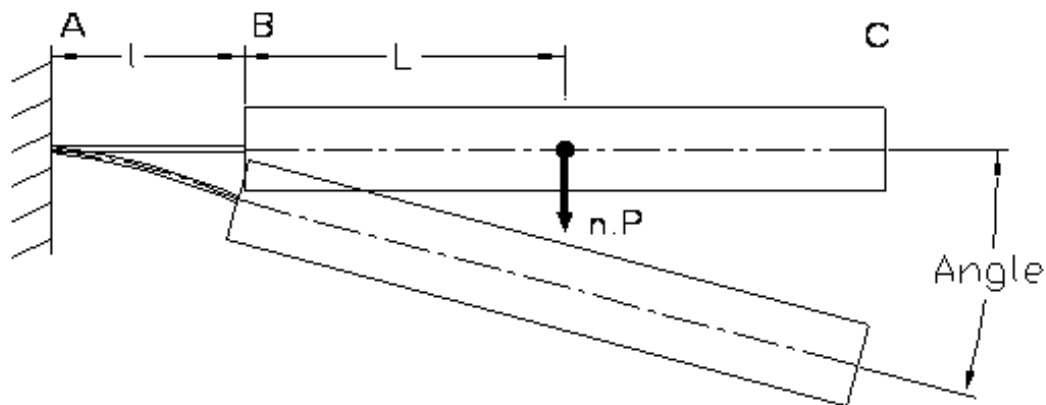


**Figure 5.1:** Static condition when centre wafer is free.

Input moment  $M = PL$ , and stress at one flexure is defined as,  $\sigma = \frac{M}{2S}$ , as here are 2 flexure with section modulus 'S', defined as  $= \frac{bh^2}{6}$  for a rectangular section (Page 135-136)

The design parameters values used for structure analysis of this centre wafer are listed in the table 5-1 below.

**Table 5-1:** Structure parameters of centre wafer

Sr. #	Parameter	Value	Units
1	Width of flexure, $b$	700	$\mu\text{m}$
2	Thickness of flexure, $h$	8	$\mu\text{m}$
3	Rigid part length from centre, $L$	2250	$\mu\text{m}$
4	Length of flexure part, $l$	800	$\mu\text{m}$
5	Total mass of pendulum part, $P$	26.8E-6	Kg
6	Tensile strength of material, $E$	7.3E4	$\text{Kg}/\text{mm}^2$

$$\text{Area moment of inertia} = \frac{bh^3}{12} = 3.4133\text{e-}008 \text{ mm}^4$$

$$\begin{aligned} \text{Stiffness, } K &= 2 \cdot \frac{EI}{l} \quad ; \text{ 2 flexure pieces of same sizes} \\ &= 0.546 \text{ g. mm / rad.} \end{aligned}$$

Stress at any flexure hinge can be calculated as

$\sigma = \frac{M}{2S}$  as here are 2 flexure with section modulus 'S' Also stress at point 'A' and point 'B' are calculated as under.

$$\sigma_B = \frac{PL}{2S} = 4.079 \text{ Kg/ mm}^2 = 40 \text{ MPa}$$

$$\sigma_A = \frac{P(L+l)}{2S} = 5.4737 \text{ Kg/ mm}^2 = 53.6 \text{ MPa}$$

Also deflection at point B & C are calculated. Deflection and angle of point 'B' in free condition is calculated as.

$$\delta_B = \frac{1}{2} \left( \frac{Pl^2}{3EI} + \frac{Pl^2}{2EI} \right) = 0.0547 \text{ mm}$$

$$\Theta = \frac{1}{2} \left( \frac{Pl}{2EI} + \frac{Pl}{EI} \right) = 0.1303 \text{ rad}$$

And maximum deflection of point 'C' in free condition is calculated as

$$\begin{aligned} \delta_C &= \delta_B + \Theta * 2L = 0.0547 + (0.1303 \times 2 \times 4.5) \text{ mm} = 0.641 \text{ mm} \\ &= 641 \mu\text{m} \end{aligned}$$

But in assembled form this maximum deflection is restricted by the fixed wafers. Maximum deflection possible in assembled form is the gap provided for capacitance pickoff. Maximum deflection possible at point 'C' in this condition is 0.010 mm (10  $\mu\text{m}$ ). Stress analysis

in the condition when centre wafer is fixed between two fixed wafers is also carried out. Maximum angle possible in this condition is 0.00189 rad.

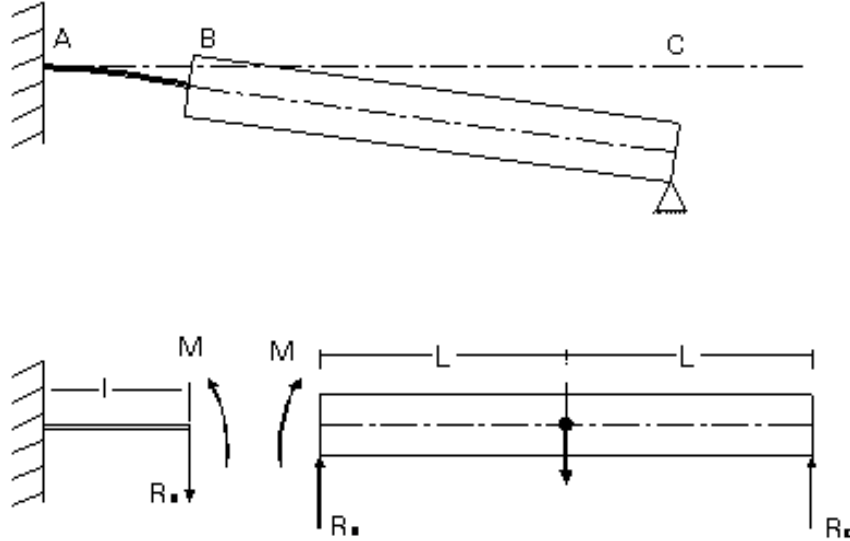


**Figure 5.2:** Static equilibrium condition when centre wafer is fixed between two wafers.

This condition is analyzed by using static equilibrium conditions and general solutions for deflection of statically determinate beams [30].

$$R_A + R_B = nP \quad \text{---} \quad 1$$

$$2L R_B + M = nPL \quad \text{---} \quad 2$$

Where 'n' is no of 'G' input

Also

$$\text{Deflection due to force} = \frac{R_B l l^2}{3EI}$$

$$\text{Deflection due to moment} = \frac{M l^2}{2EI}$$

$$\text{Angle due to force} = \frac{R_B l l}{2EI}$$

$$\text{Angle due to Moment} = \frac{Ml}{EI}$$

Applying boundary condition when deflection is = 0, Angles are converted to deflection by multiplying with length 2L.

$$\frac{R_B l l^2}{3EI} - \frac{M l^2}{2EI} + \left( \frac{R_B l l}{2EI} - \frac{Ml}{EI} \right) 2L = 0 \quad \text{---} \quad 3$$

These are three equations with three unknowns, solving these following is obtained

$$Ra = 1.4521E-005Kg$$

$$Rb = 1.2279E-005 Kg$$

$$M = 5.0452E-006Kg\text{-mm}$$

Stress due this moment 'M' is calculated  $\sigma_B = M/2S = 0.338 \text{ Kg/mm}^2(3.3 \text{ MPa})$ . This stress is produced by application of 1g input and is much less than the stress calculated in free condition. From this analysis it is concluded that in assembled form the flexures can bear much higher inputs before failure.

### 5.1.2 FEM Analysis

Stress analysis and deflection analysis is performed in COMSOL Multiphysics (FEM software) and the results are verified. Results of FEM analysis for the free condition are shown in figure 5.3. Maximum stress is at the two hinges and the stress is  $6.19E7 \text{ N/m}^2$  or 61.9MPa

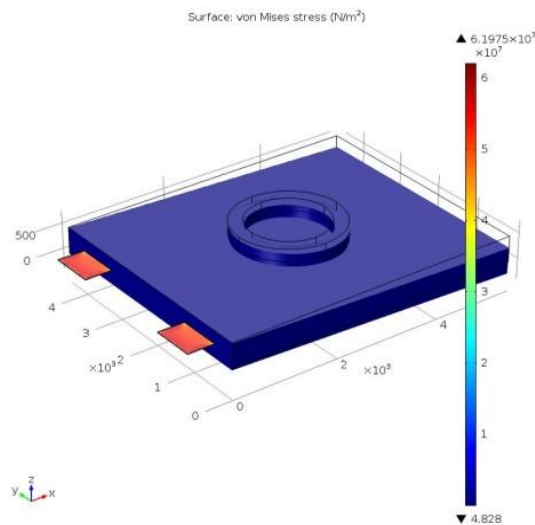


**Figure 5.3:** FEM stress analysis for free condition

Also deflection of this pendulum is through FEM analysis is compared with the deflection calculated through stiffness of flexures.

## 5.2 Magnetic Field Analysis

This accelerometer design is based on the permanent magnet based rebalance system and Lorentz force is used as a rebalance force. The Lorentz force on a wire of length L and with the

current ‘ $i$ ’ flowing in it placed in a magnetic flux density  $B$  perpendicular to the wire is given by  $F = Li \times B$ . Rebalance force is directly proportional to the magnetic field available in the working gap of coil. To get maximum required force the magnetic field and the coil placement is required to be optimized.

### 5.2.1 Magnetic Field

To get maximum magnetic field in working gap of coil a magnetic loop is designed. Also to get maximum force, magnetic field direction should be perpendicular to the current flowing through the coil. Different configurations of magnetic system with permanent magnet and soft magnet materials are proposed, performance of each is evaluated to select best possible option.

Three different configurations of magnet system are proposed as shown in figure 2.

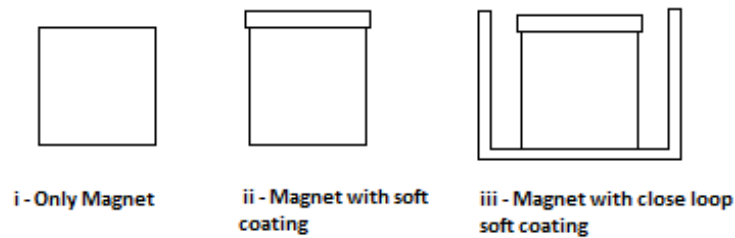


**Figure 5.4:** Three different magnet system configurations

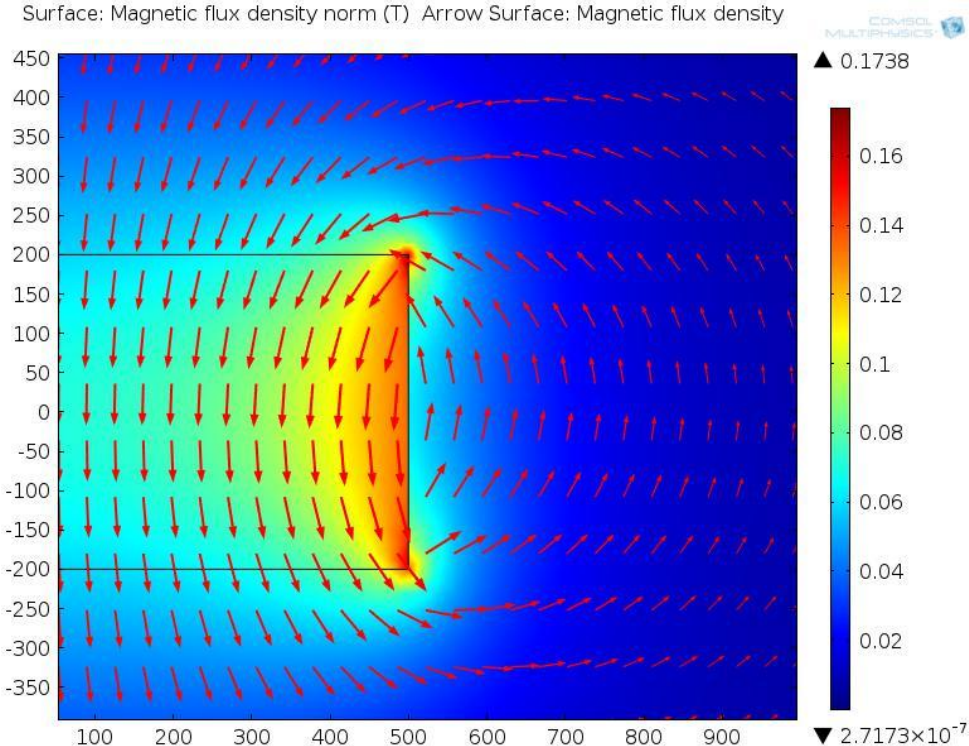
Parameters used for magnetic field simulations are given in table I.

**Table 5-2:** Simulation parameters

Sr.#	Parameter	Abrv.	Value	Units
1	Length of Magnet	lc	400	$\mu\text{m}$
2	Radius of Magnet	rm	500	$\mu\text{m}$
3	Length of Coil	lc	300	$\mu\text{m}$
4	Width of Coil Section	wc	300	$\mu\text{m}$
5	Distance b/w Coil and Magnet Centers	XX	200 ~ 500	$\mu\text{m}$
6	Magnet Saturation	Br	0.2	T

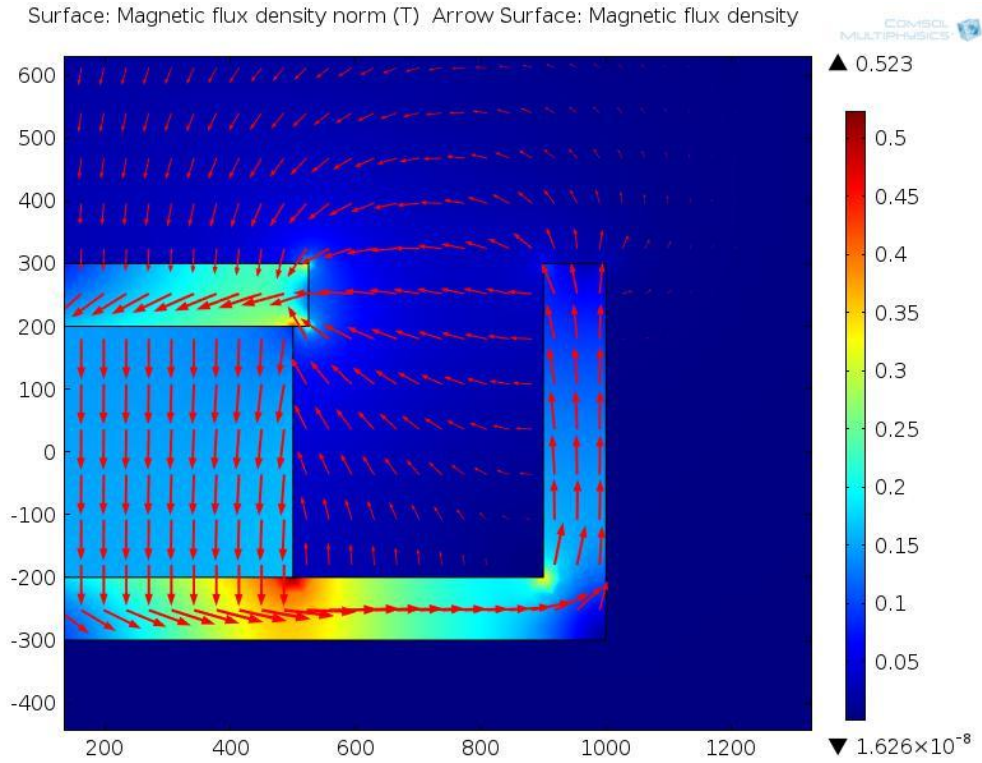
Magnetic flux density of three different proposed configurations is simulated in COMSOL Multiphysics. Variation of flux density along radius ‘ $r$ ’ and height ‘ $z$ ’ directions for all three configurations are simulated.

Fig 5.2 shows surface plot of magnetic field of configuration i (only magnet), field lines travelling from north to south in a regular way. In case of configurations ii & iii the field lines are distributed in a particular way. In configuration iii (magnet with close loop soft coating) the magnetic field lines are straight in the working gap for torque coils fig 4.



**Figure 5.5:** ThreeSurface Plot of Magnetic Field

Magnetic flux density variation along the ‘z’ direction is simulated and it is plotted from centre of magnet to 500µm for all three configurations, comparison of this is plotted in fig 5. Magnetic flux density plots show that maximum flux density is achieved in configuration-iii (magnet with close loop soft coating) and value is much higher for this configuration as compared to other two configurations due to the soft magnetic material in a close loop shape.



**Figure 5.6:** Surface plot of magnetic field

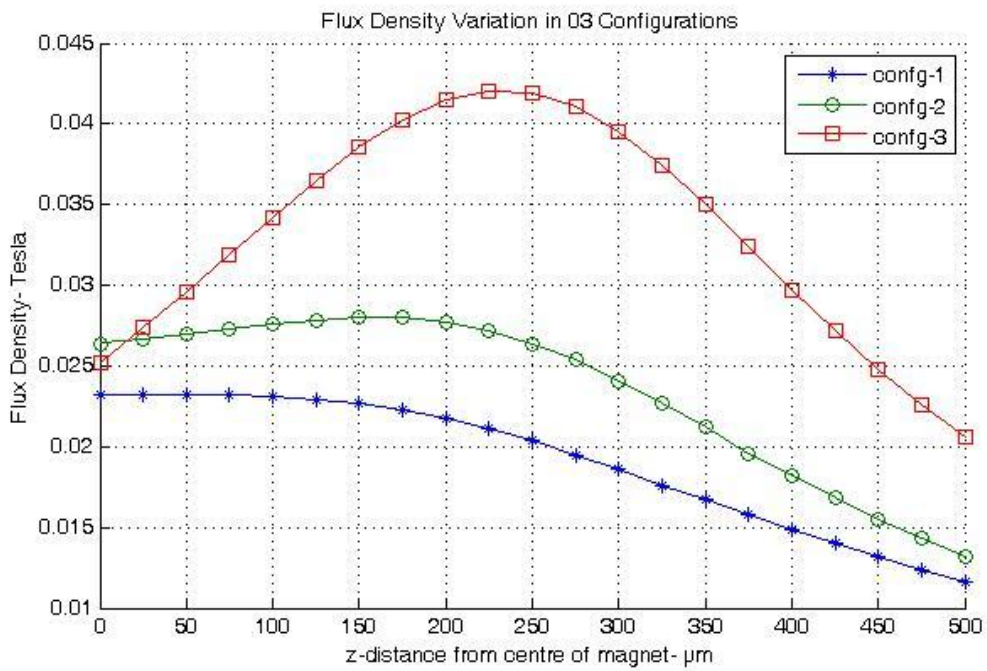


**Figure 5.7:** Magnet flux density along 'z' direction at  $r = 700 \mu\text{m}$

Also radial variation of magnetic flux density is plotted at  $z = 200 \mu\text{m}$  for configuration iii as shown in fig 6. Flux density drops sharply along radius direction but then becomes stable due to close loop configuration.

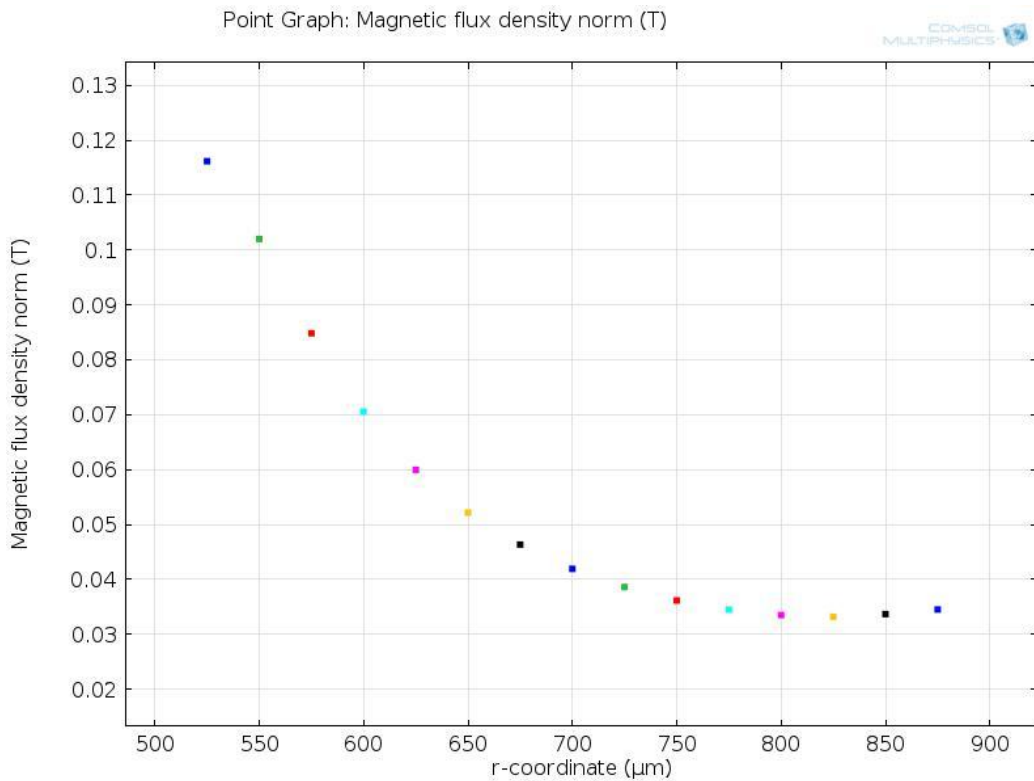


**Figure 5.8:** Magnet flux density (configuration-iii) in radial ‘r’ direction at  $z = 200 \mu\text{m}$  from centre of magnet

After magnetic flux density simulations it is concluded that configuration iii creates maximum magnetic flux density compared to other two configurations.

Further simulations are also carried out to optimize soft magnetic material coating thickness in order to get maximum magnetic field in the working gap of magnetic loop. Magnetic flux density variation with soft material thickness variation is plotted as shown in fig 8. Simulations indicates that for this configuration maximum field in the working gap can be achieved by soft material coating thickness of  $30 \sim 50 \mu\text{m}$ .



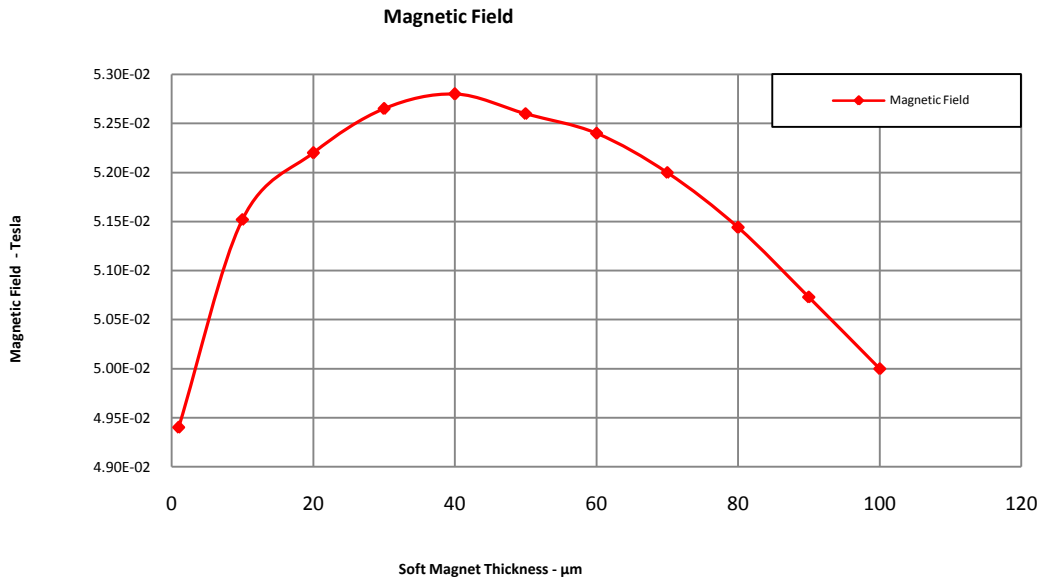


**Figure 5.9:** Soft Magnet Thickness and Magnetic Field Variation

### 5.2.2 Coil Placement

In the magnetic system under study field varies both in ‘z’ and ‘r’ directions which makes coil placement position very important in order to get maximum force.

Coil working zone is around magnet and force direction depends on the magnetization direction & current flow direction. Coil is to be placed to one side of magnet to get direction control of rebalance force. Calculation of axial force between an axial magnet and a thick coil is discussed in detail by Will Robertson ref [27]. To optimize the coil placement around magnet ‘XX’ parameter is defined from centre permanent magnet to the centre of coil shown in fig 8.

Multiple simulations are carried out in COMSOL by changing location of coil through variation of ‘XX’ in all three configurations. Electromagnetic force along z direction is plotted for three configurations. For these simulations 0.5 mA coil current is used. Results of these simulations are plotted in fig.9 for three configurations. Different force values are obtained in different configurations. Also different force peaks are observed by varying the coil placement.

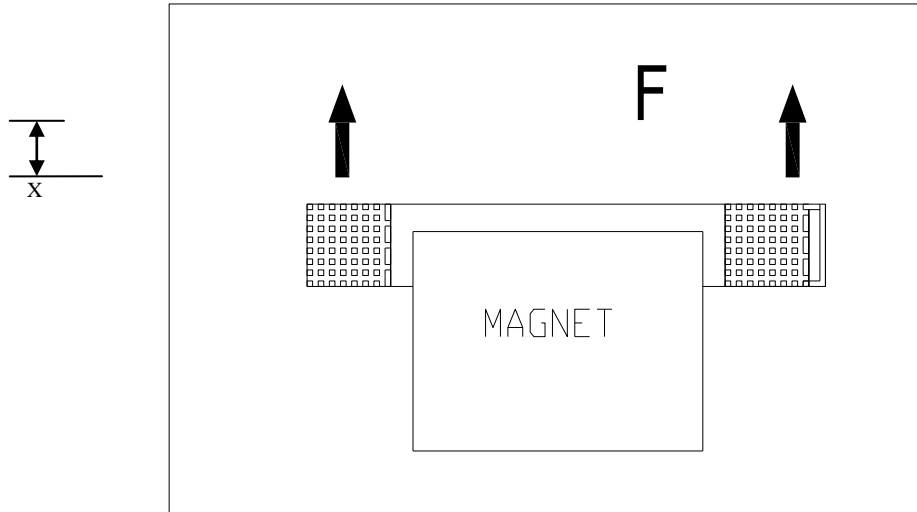


**Figure 5.10:** Force direction and distance parameter 'XX'

Maximum force is produced when magnet is used in configuration with soft magnet forming a close loop.

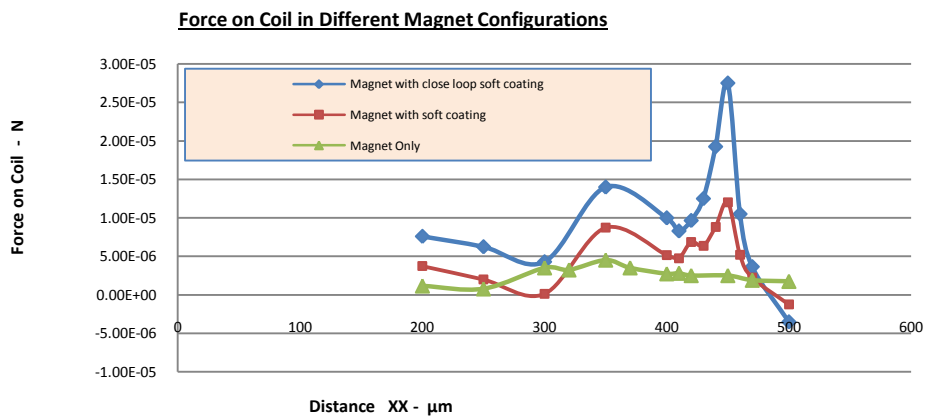


**Figure 5.11:** Force on coil, three different configurations

Although maximum force can be achieved at certain distance away from magnet but this may not be suitable option in this design due to following constraints.

- a. Maximum electromagnetic force is achieved at very precise distance which may not be possible to achieve in manufacturing/ assembly of three wafers.
- b. As coils are part of proof mass therefore slight change in position of proof mass will significantly change electromagnetic force.

It will be better to place coil near to one end of magnet and in this particular case at a centre to centre distance 'XX' of 200  $\mu\text{m}$  in order to get a stable electromagnetic force. In this magnetic MEMS accelerometer design the rebalance force required is up to 0.3 mN. To get this force complete magnetic system is designed and simulated in COMSOL. Length of magnet is 330  $\mu\text{m}$ , radius is 700  $\mu\text{m}$  and remanence  $B_r$  of only 0.25 ~ 0.3 Tesla is used. Simulations indicate that by using 144 turn coil with current of <1 mA, the required force is achieved. Surface plot of simulation are shown in fig 5.12.

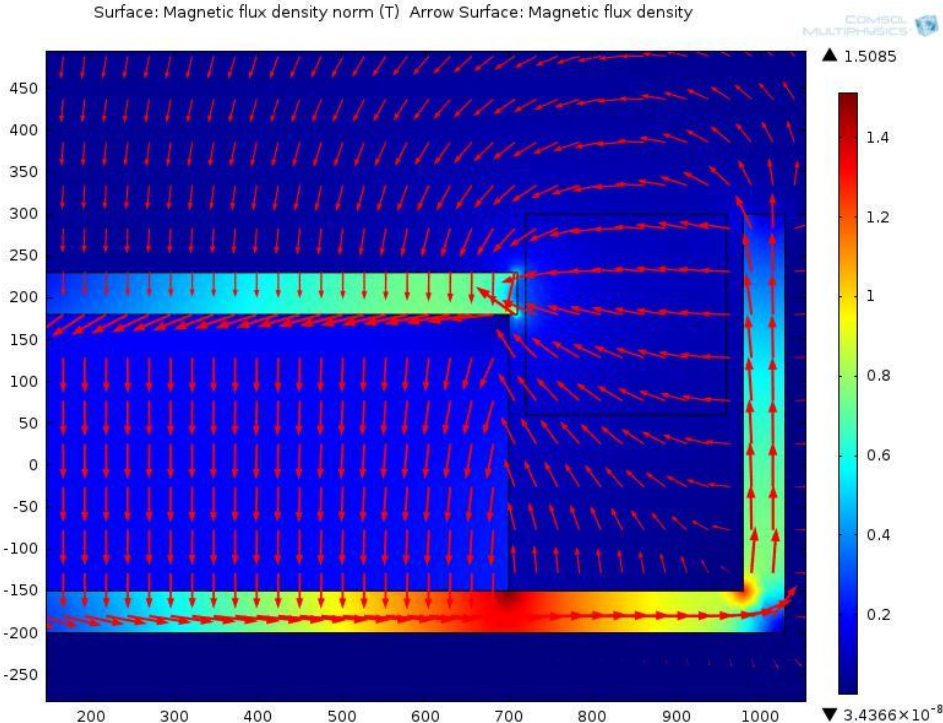


**Figure 5.12:** Surface Plot of Magnetic Field

## CHAPTER 6: FABRICATION PROCESSES

Design of this sensor system consists of three wafers as shown in figure 3.4. Three wafers will be manufactured separately and then bonded together to form a sensor. Two wafers with permanent magnet are symmetrical. Coil is fabricated on both sides of the third wafer. This third wafer is to be fixed between two wafers with permanent magnet. Fabrication processes for both magnet and proof mass coil are proposed.

Permanent magnet is the key part in this design and fabrication of permanent magnets has always been challenging in bulk batch fabrication of MEMS. Permanent magnets are produced by metallurgy process of mechanically pressing and heating. But this process is yet not compatible with MEMS production processes.

In MEMS conventionally permanent magnets are fabricated by vapor deposition methods like sputtering, evaporation, pulse laser deposition or by electrochemical deposition. By these methods a layer of only few micrometers can be deposited. Unconventional strategies like using magnetic powders of 5~50 micrometer sizes are being adopted to fabricate magnets of required size at wafer levels. Permanent magnets fabrication using magnetic powder and fabrication at wafer level is a choice for this design.

Details and performance of this method is discussed in details by Ololade D Oniku in ref [23]. Conventional deposition of micro magnets with results is described in [24,28]. Nd-Fe-B powder of size 15~ 50  $\mu\text{m}$  can be used to get the size required in this design and this can provide remanence  $B_r$  of 0.5 ~ 0.7 Tesla. Doctor's blade technique as discussed in ref [12] can be easily adopted at wafer fabrication for this design.

### 6.1 Magnet Fabrication

Permanent magnet fabrication processes are proposed here for this design. Powder fabrication technique using doctor's blade is the best suited technique available for the fabrication of required size permanent magnet in batch fabrication. Fabrication steps for complete magnetic system are described below

- Cavity etching as per dimensions of magnet and working clearance using DRIE process as shown figure 6.1(a).

- Coating of the etched cavity with soft magnet material (Ni-Fe alloy) with thickness of 30 ~ 40  $\mu\text{m}$  as shown in figure 6.1(b).
- Fill sacrificial material and then etch a cavity for permanent magnet powder fabrication as shown in figure 6.1(c).
- Permanent magnet fabrication in the cavity using powder Nd-Fe-B powder of size 15~ 50  $\mu\text{m}$  as shown in figure 6.1 (d).
- Repeat coating of soft magnet material (Ni-Fe alloy) with thickness of 30 ~ 40  $\mu\text{m}$  above the fabricated magnet as shown in figure 6.1 (e).
- Removal of all sacrificial materials to create the required working gap for rebalance coils as shown in figure 6.1(f).

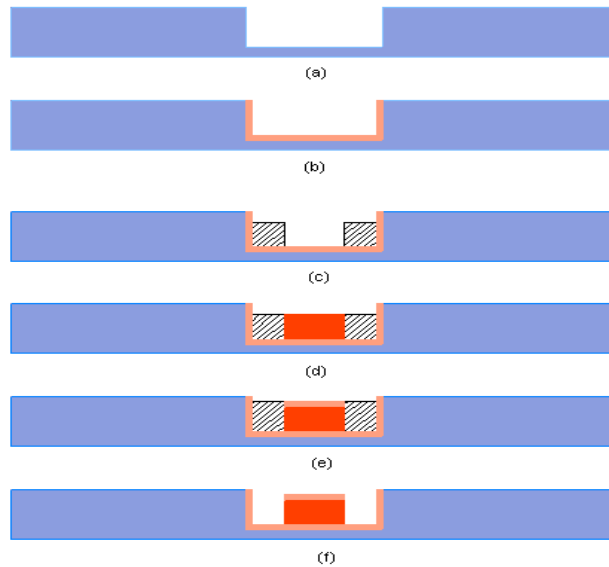


**Figure 6.1:** Magnet Fabrication process description

As only axial magnetization of the permanent magnet is required therefore magnetization of the fabricated permanent magnet wafer can be carried out in one step. Two symmetrical wafers are required for the design.

## 6.2 Flexure Fabrication

Fabrication of centre wafer is very critical. This wafer is fabricated in multiple steps. First three steps of flexure etching and capacitive coating are shown in figure 6.2 below. Fabrication of this part of wafer is described in three steps.

- Fabrication is started with wafer of thickness 500  $\mu\text{m}$ . DRIE method is suggested for etching profile of wafer. Here the profile is shown in figure 6.2(i).
- For flexure etching bulk material method is used, after masking the wafer is etched in  $\text{HF}+\text{H}_2\text{SO}_4$  solution and flexures are etched up to thickness of 8  $\mu\text{m}$  as shown in figure 6.2(ii).
- After etching and cleaning the capacitive area is thin film plated with 0.04  $\mu\text{m}$  chromium and 0.3 $\mu\text{m}$  gold by evaporation method as shown in figure 6.2(iii).

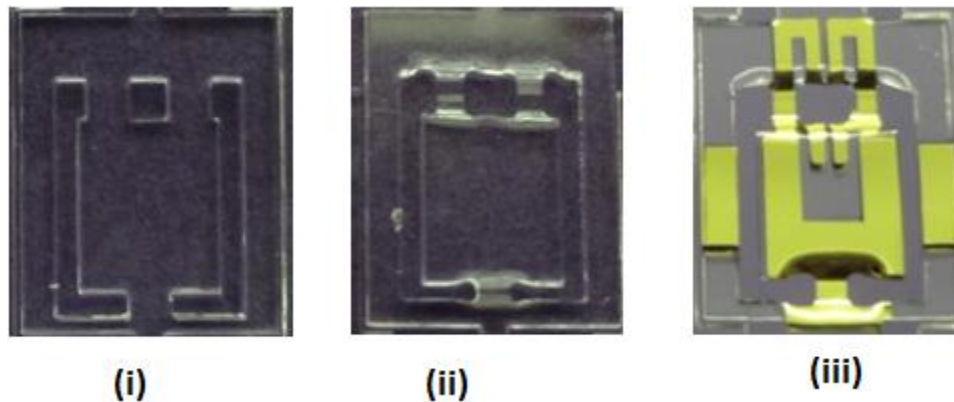


**Figure 6.2:** Flexure wafer fabrication processes (i) Etching / cutting of proof mass profile. (ii) Etching of two flexures. (iii) Thin film plating of capacitive area and connections.

### 6.3 Flexure Fabrication Stiffness Results

After fabrication of the centre wafer Stiffness of the fabricated flexure wafer is carried out. Stiffness of this wafer is carried out before coil fabrication. In this test an input moment is applied on the proof mass by tilting it by a small angle and measuring the actual deflection of proof mass. The tilt is applied using an optical indexing head of 0.1 arc sec resolution and the measurement of deflection is carried out using an autocollimator of 1arc-sec accuracy. The tilt angle provides the input force on proof mass due to gravity and the measured deflection angle of proof mass is due to its stiffness. The input force is applied in 04 different steps and deflection against each input is measure. Then average value of deflection is calculated. The results are presented in table 6-1 below. The design value of stiffness is 0.546 g-mm/rad while the measure average stiffness is 0.509 g-mm/rad. This stiffness difference between the designed value and the manufactured device is of 6.8%.

**Table 6-1:** Stiffness test results of fabricated wafer

Sr. #	Input		Measured Deflection	Stiffness
	Angle, arc-min	Moment, g-mm	Arc-sec	g-mm/rad
1	1	1.86E-5	7	0.544
2	5	9.32E-5	38	0.506
3	10	1.86E-4	78	0.49
4	20	3.73E-4	155	0.496
Average Stiffness				0.509

## 6.4 Coil Fabrication

Fabrication of rebalance coil in multi layers is required on the centre wafer. Fabrications of spiral coils have been reported and one such multi layer coil with 36 turns in two layers has been reported by Chong H Ahn, and Mark G Allen [29]. The rebalance torquer coil required in this design is of 144 turns with 12 layers. The coil spiral pattern is Cu electroplated in 12 layers with each layer separated by an insulating layer.

Fabrication steps for coil are proposed as shown in figure 6.2.

- Pattern planner spiral coil on wafer and electroplate 1<sup>st</sup> copper coil layer as shown in figure 6.2-a.
- Sputter 1<sup>st</sup> insulating layer, then pattern for two (02) copper links for the 2<sup>nd</sup> layer and electroplate copper links as shown in figure 6.2-b.
- Pattern planner spiral 2<sup>nd</sup> layer over the 1<sup>st</sup> insulating layer and electroplate 2<sup>nd</sup> copper coil layer as shown in figure 6.2-c.
- Sputter 2<sup>nd</sup> insulating layer, then pattern for two (02) copper links (different location as compared to step 'b') for 3<sup>rd</sup> layer and then electroplate copper links as shown in figure 6.2-d.
- Pattern planer spiral 3<sup>rd</sup> layer over 2<sup>nd</sup> insulating layer and then electroplate 3<sup>rd</sup> copper coil layer as shown in figure 6.2-e.
- Repeat this process to complete 12 layers of coil as shown in figure 6.2-f.
- Etching of sacrificial layers as shown in figure 6.2-g.

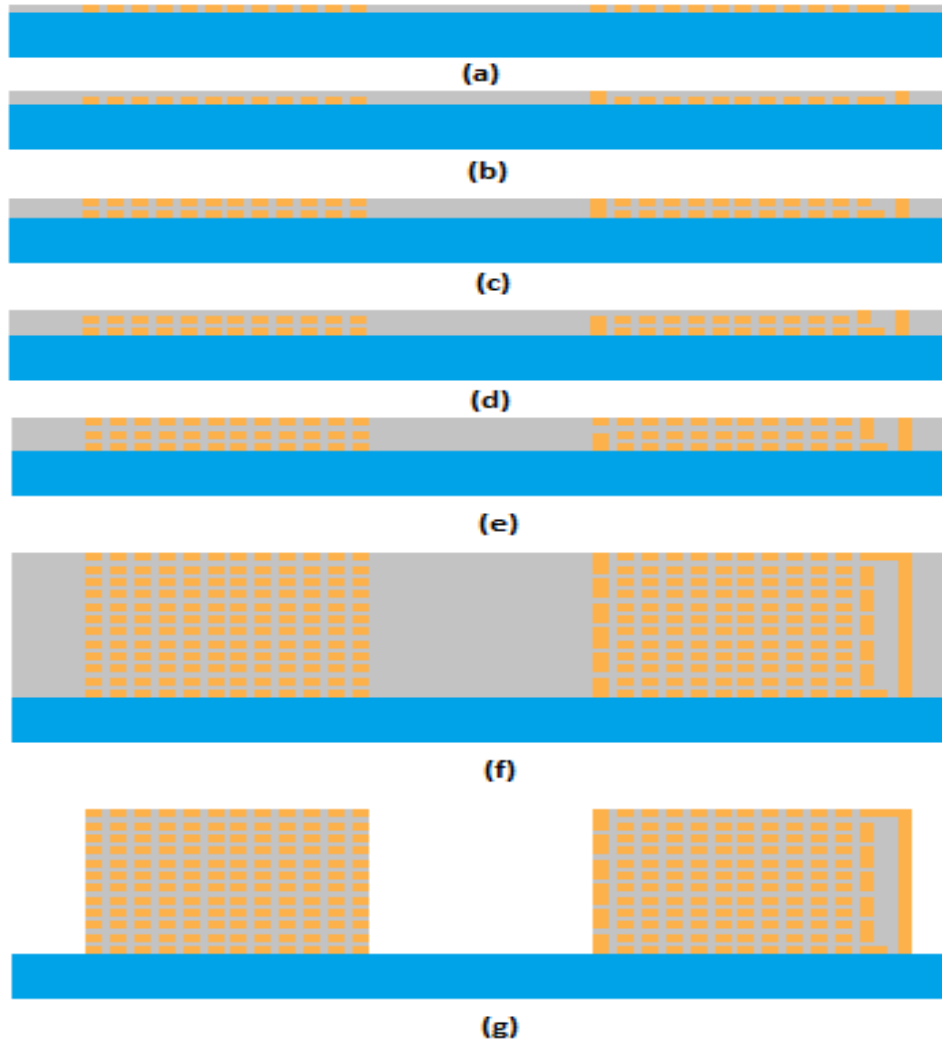
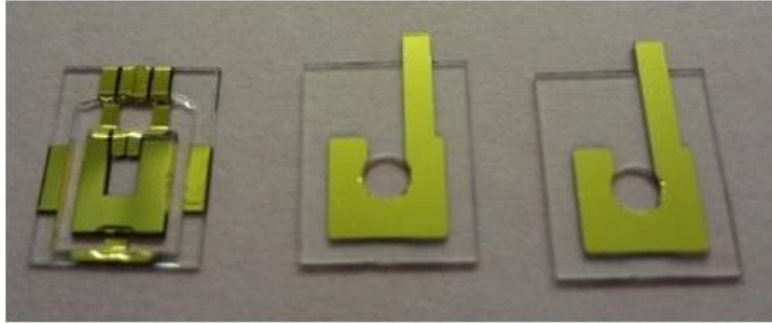


**Figure 6.3:** Coil fabrication processes

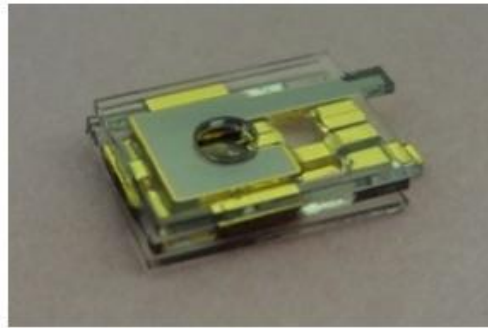
This coil is to be fabricated on both sides of wafer. Two coils are connected in series therefore via connection across wafer thickness is also made. Capacitive area coating and connection pads are connected through two flexure hinges.

Three wafers are fabricated up to a certain level (without coils and magnet fabrication) due to unavailability of facility





(i)



(ii)

**Figure 6.4:** Three wafers and device

Capacitance test of this assembled device without magnet and coils is carried out. The nominal capacitance measure of the device is 8.3 pF while the design value is 9.73pF. This difference of capacitance can be due the etching of 10 $\mu$ m capacitance distance.

## CHAPTER 7: CONTROL ANALYSIS

Close loop control analysis of proposed design with its mathematical model is carried out. Resolution, measurement range, bandwidth, non linearity and noise are the parameters to be analyzed for performance of sensor. Simulation analysis of the designed sensor is performed to find out the behavior of sensor for critical performance parameters. Measurement range is the minimum and maximum acceleration that sensor can response along its input axis with certain accuracy. As spring stiffness is designed lowest to get minimum acceleration detection, in open loop operation the small distance between the moving capacitance surface and the fixed surface limits the maximum measurement range. Performance of open loop accelerometer is very limited concerning to measurement range, bandwidth and linearity [31]. In close loop operation maximum measurement range is limited by the feedback force that can be applied to rebalance the deflected mass.

### 7.1 Close Loop Operation with Controller

This design can only be operated in closed loop with high gain pick off system with negative feedback. To achieve desired system dynamics PID controller coefficients should be carefully designed [32]. Stiffness of flexure is very small to detect smallest input. The deflection produced by smallest input is to be detected by the pickoff system. Gains of pickoff blocks are calculated to detect smallest input. Closed loop analysis of the design is performed in Matlab. Architecture of close loop with a PID controller  $H_{CONT}$  is shown in figure-7.1.

All the close loop system parameters are calculated earlier and are given in table below.

**Table 7-1:** Close loop control system parameters

Sr.#	Parameter	Abrv.	Value
1	Pickoff Angular Sensor - pF/rad	$H_{PA}$	6635
2	Pickoff Sensor Amplifier - V/pF	$H_{PSA}$	0.2
3	Time constant of Sensor Amplifier - sec	$\tau_{PSA}$	6.37E-6
4	Control Amplifier - A/V	$H_{CA}$	0.75
5	Torque Moment - g-mm/A	$H_{TM}$	80.4
6	Time constant of Torque Moment - sec	$\tau_{TM}$	5.4E-5

The parameters given in table 7.1 are used for close loop control system analysis. Steady state sensitivity of sensor depends on the mass of pendulum ‘m’, length of pendulum ‘l’ and  $K_{TM}$  of rebalance torque system. As these parameters remain constant for a sensor and for this system steady state sensitivity if calculated as  $K_{SS} = ml / K_{TM} = 0.084 / 80.4 = 0.001$  A.

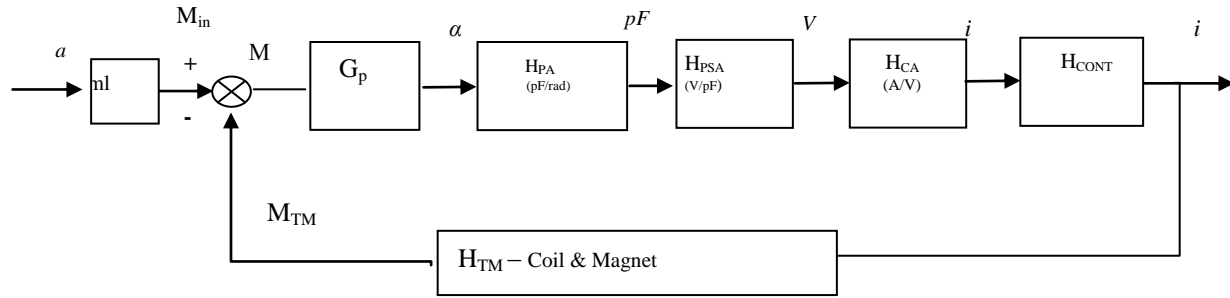


**Figure 7.1:** Close loop architecture with output configuration

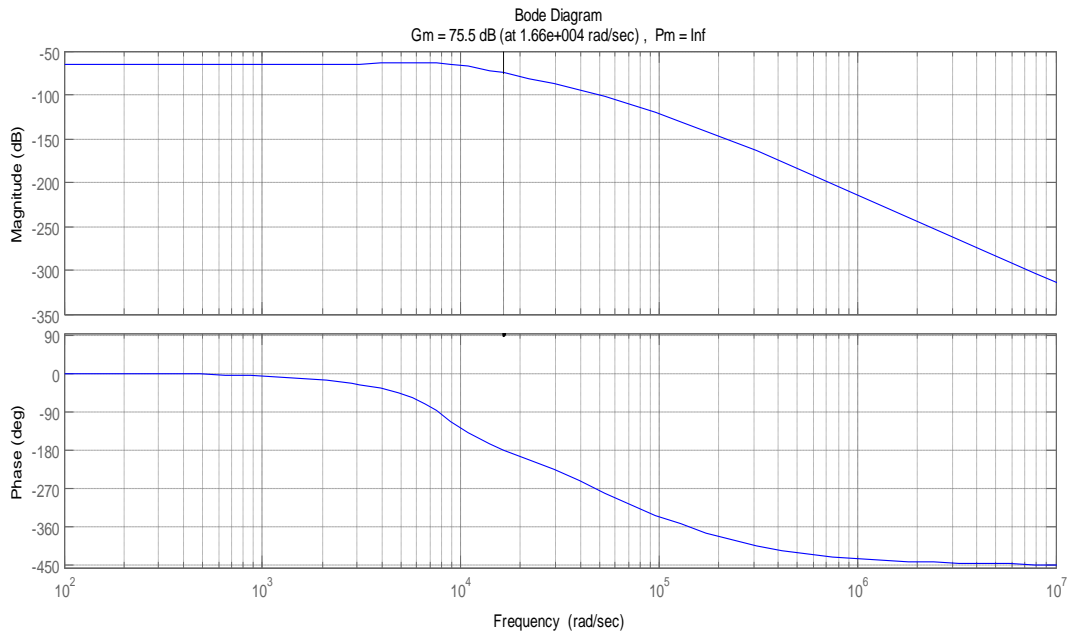


**Figure 7.2:** Frequency response plot of closed loop architecture

Frequency response analysis shows a bandwidth of  $1.03 \times 10^4$  rad/sec. Step response shows a rise time of  $1.5154 \times 10^{-4}$  sec with 20.2 % overshoot for this output configuration as is shown in figure 7.3.

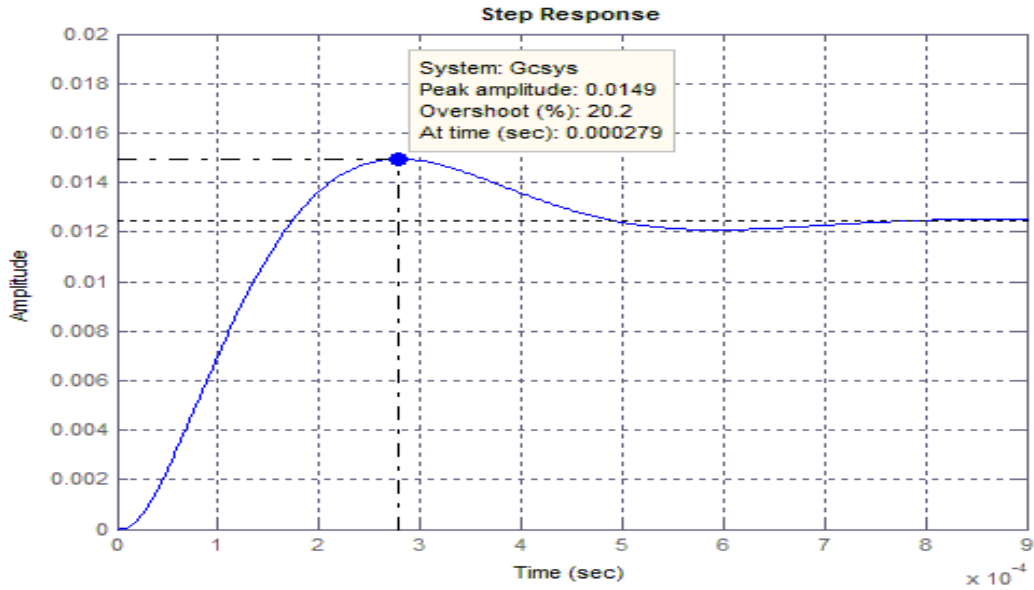


**Figure 7.3:** Step response of close loop architecture

Output response for a square input signal of 100 Hz is shown in figure 7.4

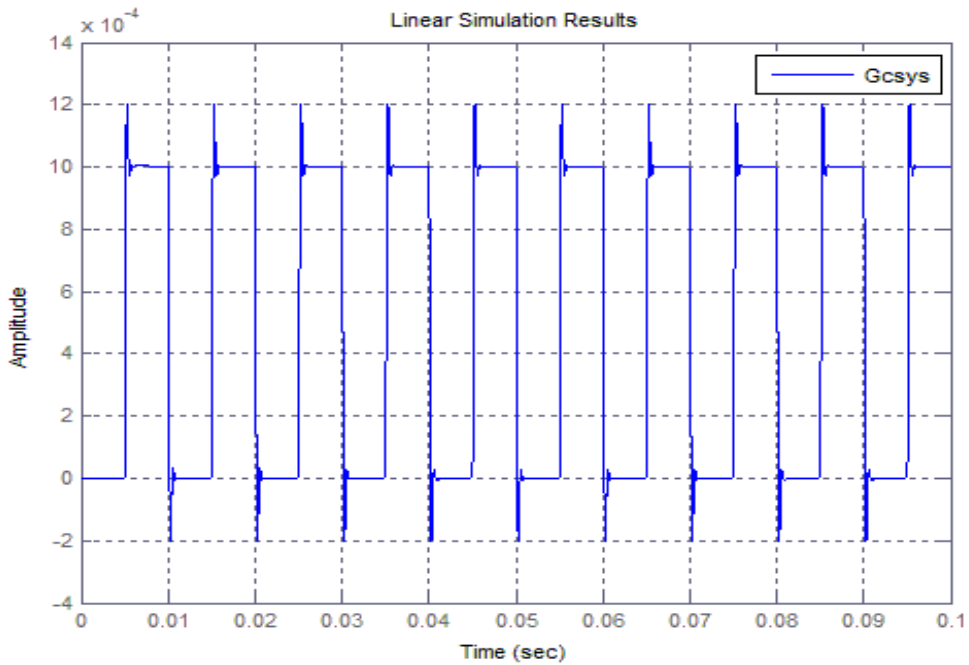


**Figure 7.4:** Response of close loop architecture at 100 Hz

An input signal at 100 Hz with multiple 'g' steps is generated as shown in figure 7.5 below. This input signal is used linear simulation analysis using Matlab and response of the system is plotted in figure 7.6.

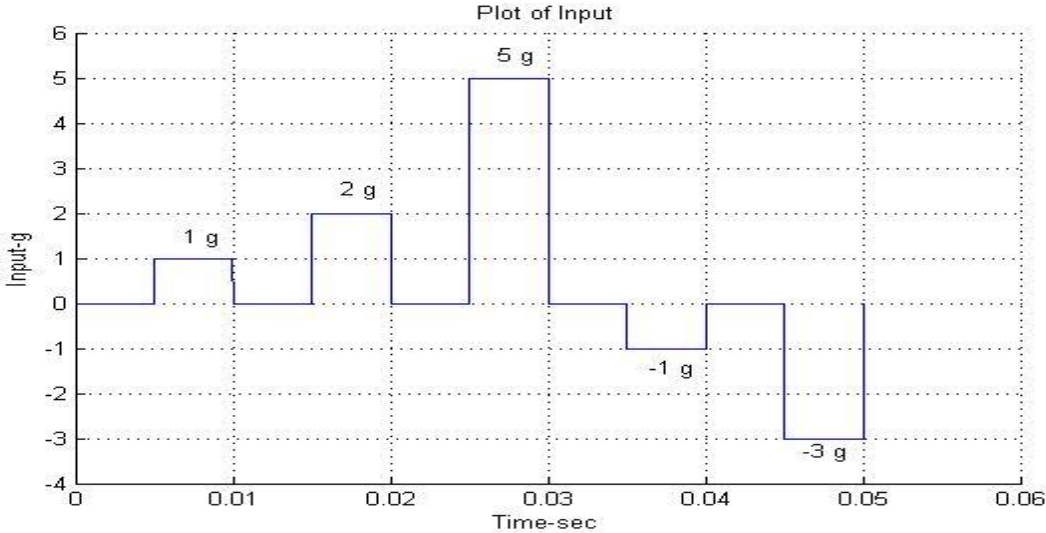


**Figure 7.5:** Input signal at 100 Hz with multiple 'g' steps

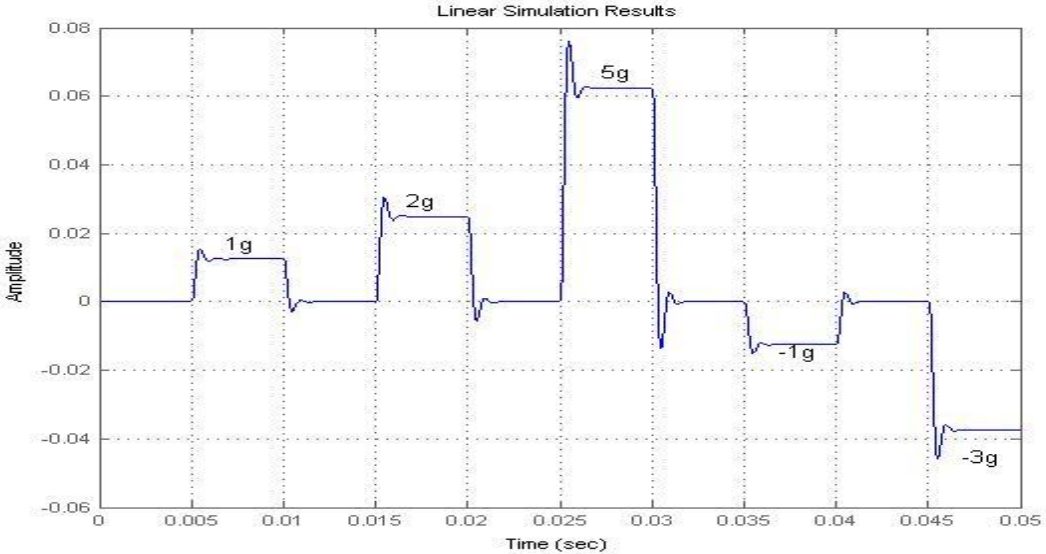


**Figure 7.6:** Response of system to Input signal at 100 Hz with multiple 'g' steps

## 7.2 Deflection Analysis

Maximum deflection of proof mass is limited by the capacitance gap. In close loop operation the deflection of proof mass must be minimum and less than the capacitance gap to avoid electrical contact. To control the angular deflection the close loop analysis is performed by transfer function as per configuration is shown in figure 7.5

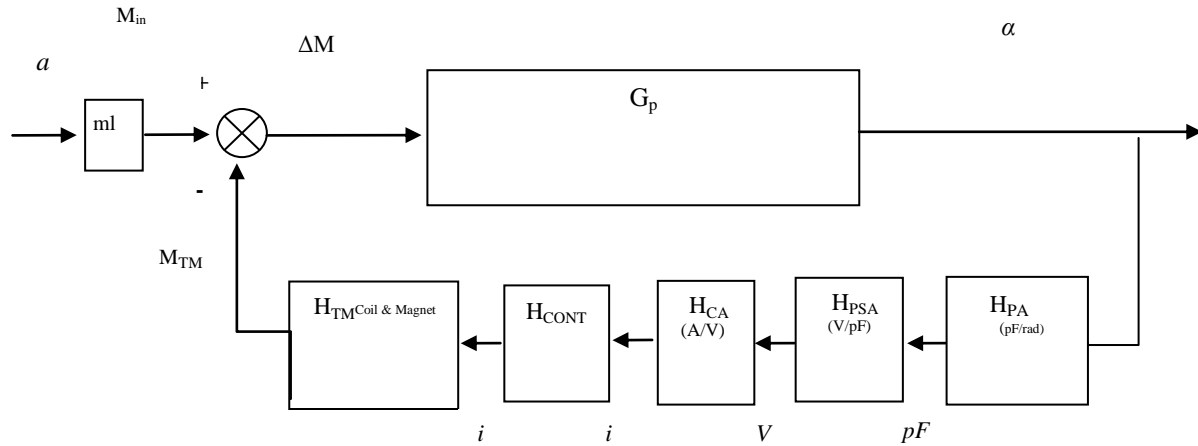


**Figure 7.7:** Close loop architecture for angular deflection

Deflection for a step input signal of different  $g$  is shown in figure-7.8. Maximum deflection at input signal of  $10\text{ g}$  is less than  $1.5 \times 10^{-3}$  rad. Minimum deflection of proof mass ensures reduced non linearity of output.

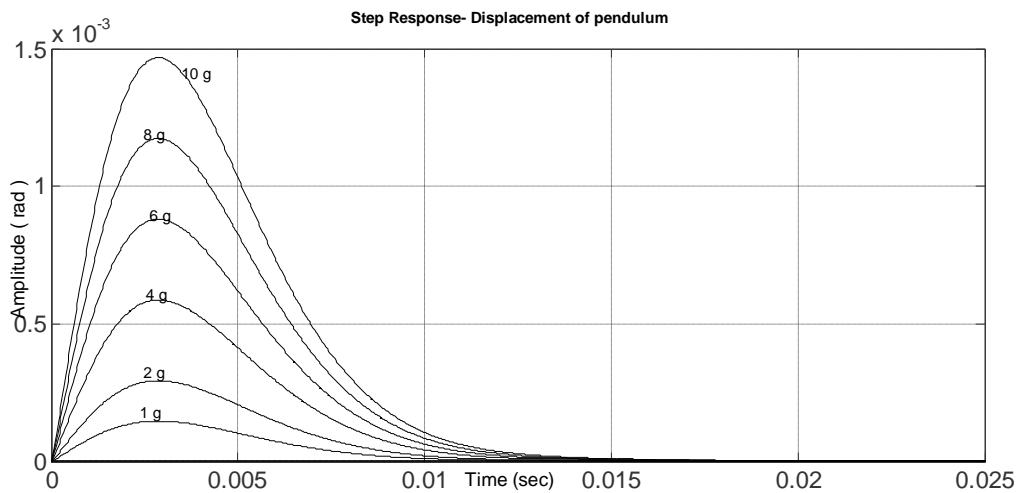


**Figure 7.8:** Deflection of sensor against step input

### 7.3 Comparison with Other Devices

Simulated performance of the device is compared with other devices especially the MEMS accelerometer by Colibrys and the traditional electromechanical accelerometers from Honeywell. Comparison of few important parameters is presented in table 7-2 below.

**Table 7-2:** Performance comparison with other devices

<b>Parameter</b>	<b>Magnetic MEMS Design</b>	<b>Colibrys</b>	<b>HONEYWELL</b>
Input Range	10 g	11.7 g	60 g
Threshold/ Resolution	10 $\mu$ g	50 $\mu$ g (MS9001)	1 $\mu$ g
Bandwidth	> 600	400	> 500
Shock Resistance	1100 g	4000 g	250 g

From this comparison it can be concluded that the performance of this designed accelerometer is better than the Colibrys device for its resolution while the input range is the same. Its shock resistance is better than the traditional accelerometer but less than the Colibrys device.

## **CONCLUSION**

The motivation and the objective of this work were to develop a high performance MEMS accelerometer that can meet the performance requirements of navigation. Navigation instrumentation of UAV,s require very space and weight reduced devices. High performance MEMS sensors are very suitable for such applications. A permanent magnet based design is proposed and analyzed for this purpose. By designing a device with partial fabrication and this control system analysis it can be concluded that an accelerometer with permanent magnet can be operated in close loop system to get a measurement range of 10g acceleration with a resolution of 10  $\mu$ g. Also a bandwidth of > 600 Hz can be achieved when operated in a close loop system.

## **FUTURE WORK**

Future work related to this accelerometer design may include

- Permanent magnet fabrication in wafers
- Spiral coil fabrication
- Electronic circuit design for this design
- PID control parameters can be further optimized to achieve close loop performance of accelerometer.



## APPENDIX A

### MATLAB PROGRAM FOR CLOSE LOOP ANALYSIS OF COMPLETE SYSTEM

```
clc
clear all
close all
pi = 3.14;
l = 0.8 ; % mm
b = 0.7 ; % mm
h = 0.008; % mm
P = 26.8e-3 ; %grams
E = 7.3e6 % gram/mm2
I = (b*h^3)/12;
row = 0.00233; % g/mm3
k = 2* E*I/l % g-mm/rad
J = 0.00002452; % g-mm-s^2
b = 0.9244 % g-mm-s

K0 = 1/k
T2 = J/k % s2
z2T = b/k %

num_G=K0;
den_G=[T2 z2T 1];
Gp=tf(num_G,den_G)
w=logspace(-1,5,1e3);
figure(1),margin(Gp);grid ;
figure(2),step(Gp);
figure(3),impulse(Gp)
H_pa = 6635 ;%pF/rad pickoff angle sensor

f= 50000; % frequency of signal Hz
K_psa = 0.2; % V/pF
tau_psa = 1/(pi*f);
H_psa = tf(K_psa,[tau_psa 1]) % psa pickoff sensor amplifier
H_ca = 0.75 ; % A/V ca Control amplifier

% controller details

Tcz = 6.0e-2; %
Tcpl = 0.1e+1; %
Tcps2 = 3e-5; %
Tcps3 = 3e-5; %

Hcz = tf([Tcz 1],1)
```

```

Hcp1 = tf(1,[Tcp1 1])
Hcp2 = tf(1,[Tcp2 1])
Hcp3 = tf(1,[Tcp3 1])

Hcont = Hcz*Hcp1*Hcp2*Hcp3

K_tm = 80.4 % g-mm/A
L = 1.6e-3; % Henry
R = 29.4; % Ohm
tau_tm = L/R;
H_tm = tf(K_tm,[tau_tm 1]) % g-mm/A

G = Gp*H_pa*H_psa*H_ca*H_tm

Gsys = Gp*H_pa*H_psa*H_ca*Hcont
Gosys = Gsys*H_tm
figure(4),margin(Gosys);grid ;
figure(5),step(Gosys)

H1 = H_pa*H_psa*H_ca;

Gcsys = feedback(Gsys,H_tm,-1)
figure(6),bode(Gcsys,w);grid ;
figure(7),margin(Gcsys);grid ;
figure(8),step(Gcsys)
hold on

[Gm,Pm,Wg,Wp] = margin(Gcsys)
figure(9);
impulse(Gcsys)
bandwidth(Gcsys)

S = stepinfo(Gcsys)
Hfed = H_pa*H_psa*H_ca*H_tm*Hcont
G2 = feedback(Gp,Hfed,-1)*0.0804
figure(10),margin(G2);grid ;
figure(11),step(G2); hold on
figure(12),impulse(G2);hold on

bandwidth(G2)
S = stepinfo(G2,'RiseTimeLimits',[0.05,0.95])

[u,t] = gensig('square',1e-2,1e-1,1e-5);

u=u*0.0804;
figure (13)
lsim(1*Gcsys,u,t)

```

```

figure (14)
lsim(Gcsys)

figure(15)
plot(t,u)

figure(16)
lsim(G2,u,t);

[u1,t1] = gensig('square',1e-2,1e-2,1e-5);

u2 = u1.*2 ;
t2 = t1+0.01+1e-5;
u3 = u1.*5 ;
t3 = t2+0.01+1e-5;

u4 = u1.*-1 ;
t4 = t3+0.01+1e-5;
u5 = u1.*-3 ;
t5 = t4+0.01+1e-5;

usteps = [u1;u2;u3;u4;u5];
tsteps= [t1;t2;t3;t4;t5];

uml=usteps*0.0804;
figure (17); hold on
xlabel('Time-sec')
ylabel('Input-g')
title('Plot of Input')
plot(tsteps,usteps); grid on

figure (18)
lsim(Gcsys)
length(tsteps)

figure (19)
lsim(G2)

```

## REFERENCES

- [1] Honeywell, Q-Flex Navigation Accelerometers, <http://www.inertialsensors.com>
- [2] Colibrys Single axis analog accelerometer <http://www.colibrys.com>
- [3] Michael Kraft “Micromachined Inertial Sensors State of the Art and a Look into the Future” University of Southampton, Highfield, Southampton, SO17 1BJ Tel: +44 (0)2380 593169, Fax: +44 (0)2380 593029, email: [mk1@ecs.soton.ac.uk](mailto:mk1@ecs.soton.ac.uk)]
- [4] Cenk Acar and Andrei M Shkel, “Experimental evaluation and comparative analysis of commercial variable-capacitance MEMS accelerometers”
- [5] Teodor Lucian Grigorie “The Matlab/Simulink Modeling and Numerical Simulation of an Analog Capacitive Micro-Accelerometer. Part1: Open loop ” MEMSTECH’ May 2008 Polyana UKRAINE
- [6] Navid Yazdi, Farrokh Ayazi, Khalil Najafi, “Micro-machined Inertial Sensors” Proceedings of IEEE Vol. 86, No. 8 Aug 1998.
- [7] R. F. Yazıcıoğlu, “Surface Micromachined Capacitive Accelerometers Using MEMS Technology”*M.S. Thesis*, Middle East Technical Univ., 2003].
- [8] V. Milanovi, E. Bowen, N. Tea, J. Suehle, B. Payne, M. Zaghloul, and M. Gaitan, “Convection-Based Accelerometer and Tilt Sensor Implemented in Standard CMOS”*Proc. Int. Mech. Eng. Conf. and Exp., MEMS Symposium*, Anaheim, Nov. 1998.
- [9] C.-H. Lui, and T. H. Kenny, “A High-Precision, Wide-Bandwidth Micromachined Tunneling Accelerometer”*J. Microelectromechanical Sys.*, Vol. 10, No. 3, pp. 425-433, Sept. 2001.
- [10] Baldwin, C., Niemczuk, J., Kiddy, J., and Slater, T. “Review of fiber optic accelerometers”, Proceedings of IMAC XXIII Conference & Exposition on Structural Dynamics, Society for Experimental Mechanics, January 31 - February 3, 2005.
- [11] B. E. Boser, “Electronics for micromachined inertial sensors” International Conference on Solid State Sensors and Actuators, 1997, vol. 2, pp. 1169 – 1172.
- [12] H. Seidel, H. Riedel, R. Kolbeck, G. Mück, W. Kupke, and M. Königer, “Capacitive silicon accelerometer with highly symmetrical design” *Sensors and Actuators: A. Physical*, 1990, vol. 21 (1-3).
- [13] E. Peeters, S. Vergote, B. Puers, and W. Sansen, “A Highly Symmetrical Capacitive Micro-Accelerometer with Single Degree-of-Freedom Response” *Transducers 91* , pp. 97-100.
- [14] B.P. van DrieEnhuizen, N.I. Maluf, I.E. Opris, and G.T.A. Kovacs, “Force-Balanced Accelerometer with mG Resolution, Fabricated using Silicon Fusion Bonding and Deep Reactive Ion Etching” International Conference on Solid-State Sensors and Actuators, Proceedings 2, 1997.
- [15] N. Yazdi and K. Najafi, “An All-Silicon Single-Wafer Fabrication Technology for Precision Microaccelerometers”, International Conference on Solid-State Sensors and Actuators, Proceedings 2, 1997.
- [16] K. -H. Han, Y. -H. Cho, "Self-balanced navigation-grade capacitive micro accelerometers using branched finger electrodes and their performance for varying sense voltage and pressure," *Journal of Microelectromechanical Systems*, 2003, vol. 12.
- [17] Y.Dong, P.Zwahlen, A.M Nguyen,R. Frosio, F. Rudolf,“ Ultra high precision MEMS accelerometer” *Transducers’11*, Beijing, China,June5-9,2011.

- [18] P. Zwahlen, Y Dong, A-M. Nguyen, F. Rudolf, J-M Stauffer, P. Ullah, V. Ragot, “Breakthrough in High Performance Inertial Navigation Grade Sigma-Delta MEMS Accelerometer”
- [19] Ralph Hopkins, Joseph Miola, Roy Setterlund, Bruce Dow, William Sawyer, “The Silicon Oscillating Accelerometer: A High- Performance MEMS Accelerometer for Precision Navigation and Strategic Guidance Application” Institute of Navigation 61st Annual Meeting Cambridge, MA, June 27-29, 2005.
- [20] Qingkun Zhou, Azhar Iqbal, Pinhas Ben-Tzavi, Dapeng Fan, “Design, Analysis, and optimization of a magnetic micro actuators” Proceedings of the ASME 2009, November 13-19 Florida, USA.
- [21] E.P Furlani, Permanent Magnet and Electromechanical Devices, Material analysis and Applications Academic press 2001.
- [22] Tsung-Shune Chin, “Permanent magnet films for application in micro-electromechanical systems” Journal of Magnetism and Magnetic Materials 209 (2000) 75-79.
- [23] Ololade D Oniku, Benjamin J Bowers, Sheetal b Shetye, Naigang Wang and David P Arnold “Permanent magnet microstructures using dry-pressed magnetic powders” Journal of Micromechanics and Microengineering published 12-june 2013.
- [24] David P. Arnold., Naigang Wang., “Permanent Magnet for MEMS”. Journal of Electromechanical Systems. Vol.18. No. 6, December 2009.
- [25] D.H.Titterton, J.L. Weston “Strapdown inertial navigation technology” 1997 Peter Peregrinus Ltd.
- [26] Ki-Ho Han , Young-Ho Cho, “ Self-Balanced Navigation-Grade Capacitive Micro-accelerometer Using Branched Finger Electrodes and Their Performance for Varying Sense Voltage and Pressure ” Journal of Microelectromechanical systems, Vol. 12, No.1, February 2003.
- [27] Will Robertson, Ben Cazzolato, Anthony Zander, “Axial Force Between a Thick Coil and a Cylindrical Permanent Magnet: Optimizing the Geometry of an Electromagnetic Actuator” IEEE Transactions on Magnetics Vol. 48 No.9, September 2012.
- [28] Paul McGuinness David Jezersek, Spomenka Kobe, “100-  $\mu$ -thick Nd-Fe-B magnets for MEMS applications produced via a low-temperature sintering route.”
- [29] Chong H. Ahn, Mark G. Allen. “Micro- machined Planar Inductors on Silicon Wafers for MEMS Applications”. IEEE Transactions on Industrial Electronics Vol. 45, No.6 December 1998.
- [30] Andrew Pytel, Ferdinand L. Singer, “Strength of Materials”
- [31] Teodor Lucian Grigorie “The Matlab/Simulink Modeling and Numerical Simulation of an Analog Capacitive Micro-Accelerometer. Part2: Closed loop” MEMSTECH’ May 2008 Polyana UKRAINE
- [32] Yin Liang, Liu Xiaowei, Chen Weiping, Zhou Zhiping, “High resolution interface circuit for closed-loop accelerometer” Journal of semiconductor Vol.32, No.4 April 2011.